Fermilab

S^5: Tidal Disruption in Crater 2 and Formation of Diffuse Dwarf Galaxies in the Local Group

FERMILAB-PUB-25-0952-PPD

arXiv:2512.02177

Draft version December 3, 2025
Typeset using LaTeX **twocolumn** style in AASTeX62

S^5: Tidal Disruption in Crater 2 and Formation of Diffuse Dwarf Galaxies in the Local Group

Guilherme Limberg,[1,2] Alexander P. Ji,[2,1,3] Ting S. Li,[4,5,6] Denis Erkal,[7] Sergey E. Koposov,[8,9] Andrew B. Pace,[10,*] Andrew P. Li,[5] Petra Awad,[11] Alexandra Senkevich,[12] Joss Bland-Hawthorn,[13] Lara Cullinane,[14] Gary Da Costa,[15] Alex Drlica-Wagner,[2,1,16,3] Raphaël Errani,[17] Peter S. Ferguson,[18] Kyler Kuehn,[19] Geraint F. Lewis,[13] Sarah L. Martell,[20] Jorge Peñarrubia,[8] Nora Shipp,[18] Yong Yang,[13] and Daniel B. Zucker[21,22]
(S^5 Collaboration)

[1] *Kavli Institute for Cosmological Physics, University of Chicago, 5640 S. Ellis Avenue, Chicago, IL 60637, USA*
[2] *Department of Astronomy & Astrophysics, University of Chicago, 5640 S. Ellis Avenue, Chicago, IL 60637, USA*
[3] *NSF-Simons AI Institute for the Sky (SkAI), 172 E. Chestnut St., Chicago, IL 60611, USA*
[4] *Department of Astronomy and Astrophysics, University of Toronto, 50 St. George Street, Toronto, ON M5S 3H4, Canada*
[5] *Dunlap Institute for Astronomy & Astrophysics, University of Toronto, 50 St. George Street, Toronto, ON M5S 3H4, Canada*
[6] *Data Sciences Institute, University of Toronto, 17th Floor, Ontario Power Building, 700 University Avenue, Toronto, ON M5G 1Z5, Canada*
[7] *School of Mathematics and Physics, University of Surrey, Guildford GU2 7XH, UK*
[8] *Institute for Astronomy, University of Edinburgh, Royal Observatory, Blackford Hill, Edinburgh EH9 3HJ, UK*
[9] *Institute of Astronomy, University of Cambridge, Madingley Road, Cambridge CB3 0HA, UK*
[10] *Department of Astronomy, University of Virginia, 530 McCormick Road, Charlottesville, VA 22904, USA*
[11] *Leiden Observatory, Leiden University, PO Box 9513, NL-2300 RA Leiden, The Netherlands*
[12] *Department of Physics, University of Surrey, Guildford GU2 7XH, UK*
[13] *Sydney Institute for Astronomy, School of Physics, A28, The University of Sydney, NSW 2006, Australia*
[14] *Leibniz-Institut für Astrophysik Potsdam (AIP), An der Sternwarte 16, D-14482 Potsdam, Germany*
[15] *Research School of Astronomy and Astrophysics, Australian National University, Canberra, ACT 2611, Australia*
[16] *Fermi National Accelerator Laboratory, P.O. Box 500, Batavia, IL 60510, USA*
[17] *McWilliams Center for Cosmology and Astrophysics, Department of Physics, Carnegie Mellon University, 5000 Forbes Avenue, Pittsburgh, PA 15213, USA*
[18] *DIRAC Institute, Department of Astronomy, University of Washington, 3910 15th Ave NE, Seattle, WA, 98195, USA*
[19] *Lowell Observatory, 1400 W Mars Hill Rd, Flagstaff, AZ 86001, USA*
[20] *School of Physics, University of New South Wales, Sydney, NSW 2052, Australia*
[21] *School of Mathematical and Physical Sciences, Macquarie University, Sydney, NSW 2109, Australia*
[22] *Macquarie University Research Centre for Astrophysics and Space Technologies, Sydney, NSW 2109, Australia*

ABSTRACT

We present results of a spectroscopic campaign around the diffuse dwarf galaxy Crater 2 (Cra2) and its tidal tails as part of the Southern Stellar Stream Spectroscopic Survey (S^5). Cra2 is a Milky Way dwarf spheroidal satellite with extremely cold kinematics, but a huge size similar to the Small Magellanic Cloud, which may be difficult to explain within collisionless cold dark matter. We identify 143 Cra2 members, of which 114 belong to the galaxy's main body and 29 are deemed part of its stellar stream. We confirm that Cra2 is dynamically cold (central velocity dispersion $2.51^{+0.33}_{-0.30}$ km s^{-1}) and also discover a $\approx 7\sigma$ velocity gradient consistent with its tidal debris track. We separately estimate the stream velocity dispersion to be $5.74^{+0.98}_{-0.83}$ km s^{-1}. We develop a suite of N-body simulations with both cuspy and cored density profiles on a realistic Cra2 orbit to compare with S^5 observations. We find that the velocity dispersion ratio between Cra2 stream and galaxy ($2.30^{+0.41}_{-0.35}$) is difficult to reconcile with a cuspy halo with fiducial concentration and an initial mass predicted by standard stellar mass–halo mass relationships. Instead, either a cored halo with relatively small core radius or a low-concentration cuspy model can reproduce this ratio. Despite tidal mass loss, Cra2 is metal-poor ($\langle$[Fe/H]$\rangle = -2.16 \pm 0.04$) compared to the stellar mass–metallicity relation for its luminosity. Other diffuse dwarf galaxies similar to Cra2 in the Local Group (Antlia 2 and Andromeda 19) also challenge galaxy formation models. Finally, we discuss possible formation scenarios for Cra2, including ram-pressure stripping of a gas-rich progenitor combined with tides.

Corresponding author: Guilherme Limberg
limberg@uchicago.edu

Keywords: Dark matter; Local Group; dwarf galaxies; low surface brightness galaxies; stellar streams

1. INTRODUCTION

Dwarf galaxies occupy the extreme low-mass end of the galaxy luminosity function (e.g., Koposov et al. 2008; Drlica-Wagner et al. 2020; Tan et al. 2025). These are the most chemically pristine and dark-matter dominated systems in the Universe (Tolstoy et al. 2009; Simon 2019). Their stellar populations provide insights on the drivers of galaxy evolution at small scales (Sales et al. 2022) and their internal dynamics are sensitive to the physics of dark matter (Battaglia & Nipoti 2022). Therefore, understanding the assembly of dwarf galaxies is critical to achieve a complete understanding of the multi-scale process of galaxy formation through the interplay between baryons and their hosting dark matter halos (Wechsler & Tinker 2018).

Crater 2 (Cra2) is a Milky Way (MW) dwarf spheroidal (dSph) satellite and one of the most diffuse galaxies ever identified (Torrealba et al. 2016). This faint dwarf galaxy has a size (circularized half-light radius; $R_{1/2}$) similar to the Small Magellanic Cloud (SMC; Muñoz et al. 2018, $\sim$1 kpc), but $\sim$1000$\times$ lower stellar mass[23]. Its huge size and cold line-of-sight velocity dispersion ($\sigma_v \sim 2.5$ km s^{-1}; Caldwell et al. 2017; Ji et al. 2021) make Cra2 one of the most severe outliers in the scaling relation between σ_v and $R_{1/2}$, i.e., a proxy for the mass–size relation (e.g., Walker et al. 2010, and see Errani et al. 2022 for a recent version), in the Local Group (see left panel of Figure 1). The old stellar population (>10 Gyr; Walker et al. 2019) and lower-than-expected metallicity for its luminosity (Ji et al. 2021) add to the remarkable properties of Cra2.

Galaxy evolution within collisionless cold dark matter (CDM) does offer a natural way to enlarge galaxies via tidal disruption (Peñarrubia et al. 2008; Errani et al. 2015). However, even with tides, dynamical N-body simulations of 'cuspy' Navarro-Frenk-White (NFW) halos (Navarro et al. 1996b, 1997) struggle to reconcile Cra2's large $R_{1/2}$ with its tiny σ_v (Sanders et al. 2018; Borukhovetskaya et al. 2022; Errani et al. 2022). A possible solution is to invoke that Cra2 is embedded in an NFW halo with either an unusually low concentration (see Amorisco 2019) or extremely low halo mass for its luminosity. Another possibility is that Cra2 inhabits a 'cored' halo instead, with a constant central density (e.g., de Blok 2010), which would allow for extra enlargement and suppression of σ_v for a fixed amount of mass loss (Fu et al. 2019). The issue with this hypothesis is that Cra2's stellar mass ($M_\star \sim 3 \times 10^5\, M_\odot$) is not large enough for energetic supernovae feedback to destroy its central cusp and create a core (see review by Bullock & Boylan-Kolchin 2017).

As an alternative to a cored dark matter halo, results from hydrodynamical cosmological simulations imply that extreme $M_\star$ loss, perhaps $\sim$99%, could reproduce Cra2's structural properties even in the normal-concentration NFW case (Fattahi et al. 2018; Applebaum et al. 2021). However, since Cra2 is metal-poor compared to the Local Group's stellar mass–metallicity relation (MZR; Kirby et al. 2013; Simon 2019), this argument has been mostly rejected since a tidally disrupted galaxy should appear to be metal-rich instead (Ji et al. 2021, and see discussion by Riley et al. 2025), as is the case for Sagittarius dSph (e.g., Hayes et al. 2020).

Given the lack of a satisfactory mechanism to fabricate galaxies like Cra2, we face the exciting possibility that a modification to the CDM model might be required. For example, self-interacting dark matter, where (postulated) dark matter particles can scatter and thermalize (Spergel & Steinhardt 2000), might be able to explain Cra2's structural properties, including both size and velocity dispersion (Kahlhoefer et al. 2019; Lovell & Zavala 2023; Zhang et al. 2024). Tidal stripping with fuzzy (or wave) dark matter, where the quantum uncertainty principle itself creates a constant density core in dwarf galaxies (Hu et al. 2000; Schive et al. 2014), might also reproduce Cra2's extended morphology and cold kinematics (Pozo et al. 2022). We note, however, that this scenario has already been strongly constrained by dwarf kinematics itself (Dalal & Kravtsov 2022). Lastly, Modified Newtonian Dynamics (Milgrom 1983) correctly predicts Cra2's σ_v value to be between $\sim$1.5 km s^{-1} and 3.0 km s^{-1} (McGaugh 2016), although such model is unable to reproduce large-scale structure formation.

Despite its extraordinary properties, Cra2 is not completely unique in the Local Group. Both the MW satellite Antlia 2 (Ant2; Torrealba et al. 2019) and M31 satellite Andromeda 19 (And19; McConnachie et al. 2008) display comparable properties, such as extended morphology, cold kinematics, old stellar populations, and low metallicity (e.g., Collins et al. 2020, 2022; Ji et al. 2021). These nearby diffuse dwarfs resemble external "ultra-diffuse" galaxies (UDGs; van Dokkum et al. 2015; Koda et al. 2015) usually found in dense cluster en-

* Galaxy Evolution and Cosmology (GECO) Fellow

[23] Assuming the mean stellar mass-to-light ratio values from Woo et al. (2008) for star-forming ($1.0\, M_\odot/L_\odot$) and quenched ($1.6\, M_\odot/L_\odot$) dwarf galaxies for SMC and Cra2, respectively.

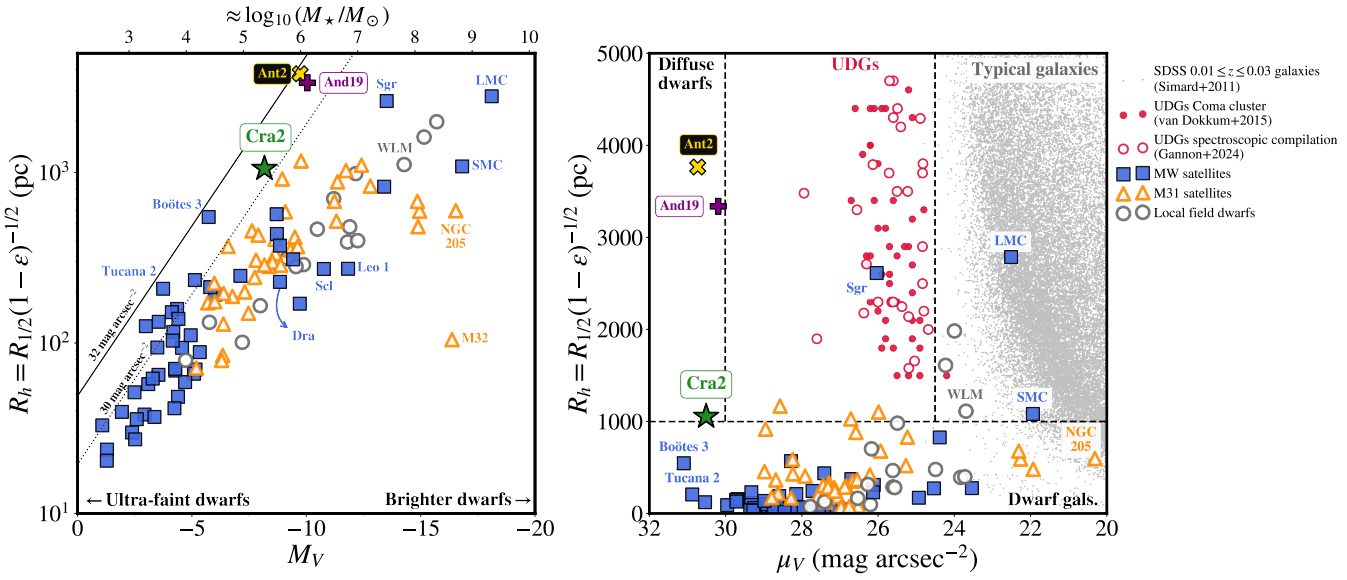

Figure 1. Left: absolute V-band magnitude (M_V) vs. size diagram for Local Group dwarf galaxies (compilation by Pace 2025). The vertical axis corresponds to the half-light major axis $R_h = R_{1/2}(1-\epsilon)^{-1/2}$, where $R_{1/2}$ is the circularized half-light radius and ϵ is the ellipticity. The corresponding stellar masses ($M_\star$) are computed as in Equation 5. Diagonal lines exhibit constant values of surface brightness following annotations. Diffuse dwarfs Crater 2 (green '⋆' symbol), Antlia 2 (yellow 'X'), and Andromeda 19 (purple '+') are highlighted. Milky Way satellites, M31 satellites, and Local Group field dwarf galaxies are plotted as blue squares, orange triangles, and gray circles, respectively. Right: V-band surface brightness (μ_V) vs. size (R_h). Ultra-diffuse galaxies (UDGs) in the Coma cluster (van Dokkum et al. 2015) are shown as the red dots. White circles with red edges represent other UDGs from a spectroscopic compilation (Gannon et al. 2024). Gray dots are typical galaxies from the Sloan Digital Sky Survey data release 7 within the redshift range $0.01 \leq z \leq 0.03$ (Simard et al. 2011, and references therein).

vironments (van der Burg et al. 2017). Having said that, Cra2 and its siblings are much more extreme and lower-mass systems than UDGs; these local dwarfs are ∼100× more diffuse than the prototypical UDG population (right panel of Figure 1). Nevertheless, UDGs raise similar concerns, and solutions, regarding their possible formation pathway(s) (Di Cintio et al. 2017; Carleton et al. 2019; Mancera Piña et al. 2019; Kong et al. 2022; Nadler et al. 2023; Benavides et al. 2023).

The leading hypotheses, either within or outside CDM, for the formation of Cra2, and its analogs Ant2 and And19, require tidal disruption. Coppi et al. (2024) recently detected a linear overdensity of variable RR Lyrae (RRL) stars around Cra2. This stellar stream aligns with the on-sky proper motion vector of Cra2 and strongly suggests that this dwarf galaxy is indeed experiencing heavy tidal mass loss. In this paper, we investigate the chemodynamical properties of Cra2 and its stellar stream with red giant-branch (RGB) stars observed as part of the Southern Stellar Stream Spectroscopic Survey (S^5) program (Li et al. 2019). We explore the kinematics of the Cra2 stellar stream to infer properties of its dark matter density profile. The chemistry along the Cra2 stream will also inform us, for example, if the most metal-poor stellar population has been preferentially stripped, which would have implications for the mass–metallicity relation.

This paper is organized as follows. In Section 2, we describe the S^5 data. Methods and quantitative results are presented in Sections 3 and 4, respectively. Section 5 is dedicated to discussing formation channels for Cra2 in the context of our findings. Finally, conclusions and a brief summary are provided in Section 6.

2. DATA

This paper utilizes data from the forthcoming S^5 second data release (DR2; T. S. Li et al., in preparation)[24]. The main science goal for S^5 is to characterize the kinematics and chemistry of stellar streams. For this, S^5 performs dedicated follow-up observations of known stellar stream fields with the dual-arm AAOmega spectrograph (Sharp et al. 2006) coupled with the Two-degree Field (2dF) fibre positioner (Lewis et al. 2002) at the 3.9 m Anglo-Australian Telescope. S^5 initiated its program mid-2018 by targeting stellar streams identified in the Dark Energy Survey (Shipp et al. 2018, and references therein). Since then, S^5 has expanded to include several other stellar streams found in the Southern sky (e.g., Li

[24] This corresponds to the internal release iDR3.7.

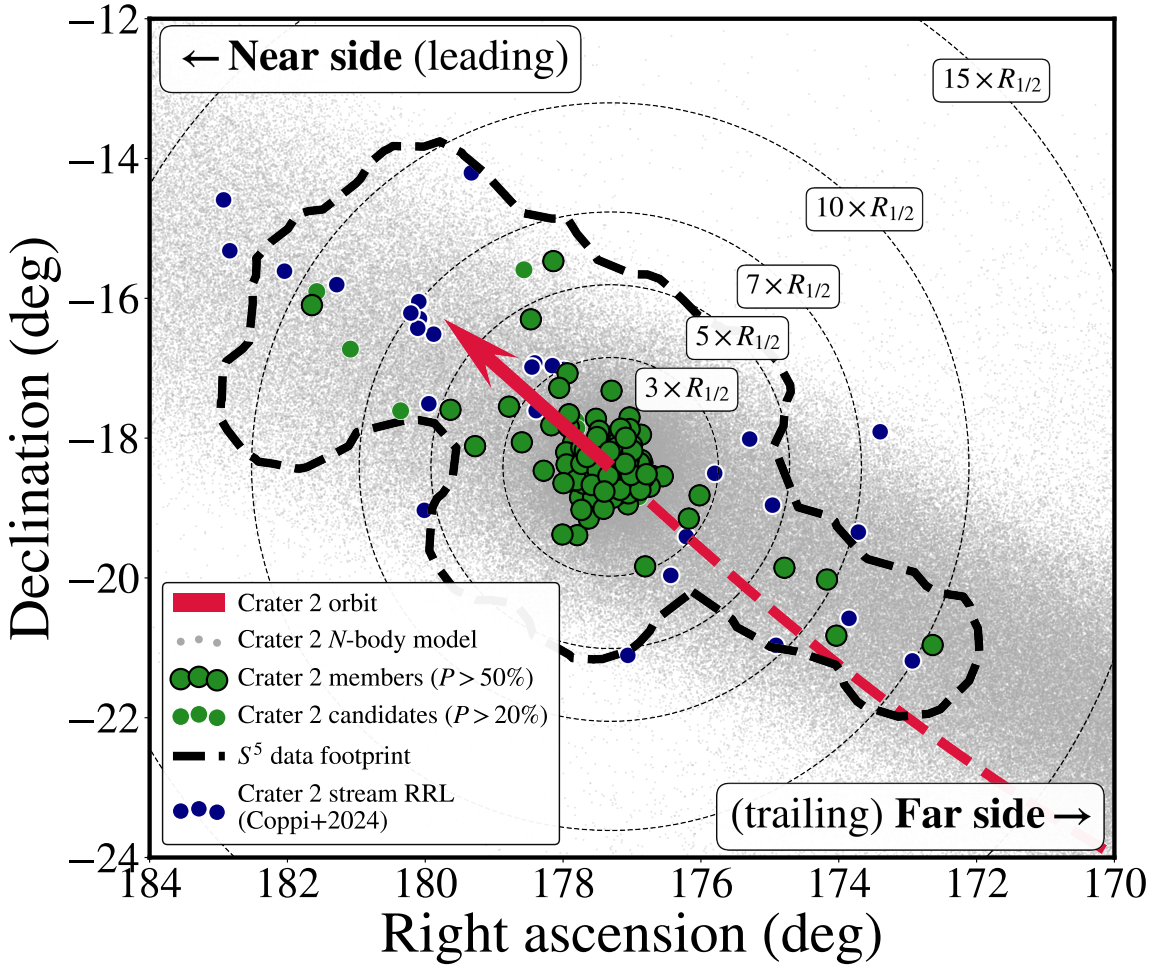

Figure 2. On-sky stellar spatial distribution around the Crater 2 (Cra2) galaxy. Green circles with black edges are S^5 Cra2 members with a probability $P > 50\%$ from our mixture model (Section 3.3), including remnant body and stream. Other Cra2 candidates ($20\% < P \leq 50\%$) are shown as the smaller green dots. Variable RR Lyrae stars in the Cra2 stream are displayed as the dark blue circles with white edges (Coppi et al. 2024). The directions of both "far side" ($\alpha \lesssim 177.5°$) and "near side" ($\alpha \gtrsim 177.5°$) of the stream are annotated. The 2dF+AAOmega fields observed as part of S^5 are presented as the dashed black contour. The thin dotted lines mark 3, 5, 7, 10, and 15 $R_{1/2}$ around Cra2, where $R_{1/2} = 31.2$ arcmin with a null ellipticity (Torrealba et al. 2016). The Cra2 `core-base` N-body model star particles (Section 3.1) are the gray dots in the background. Finally, the red arrow and dashed line exhibit the Cra2 proper motion vector in Galactic standard of rest frame and its past orbit used for the N-body simulations, respectively.

et al. 2022) as well as surviving, but tidally disrupting, dwarf galaxies and globular clusters.

In total, S^5 has observed 14 fields of $\sim$3 deg^2 each around the center of Cra2 and along the predicted track for its stripped debris using the 2dF+AAOmega combination (Figure 2). Indeed, this debris track does coincide with the Cra2 stream detected by Coppi et al. (2024) with RRL stars. The central Cra2 field has been observed twice during February 2020 and the collected S^5 data have already been published in Ji et al. (2021). Two additional pointings with 2dF+AAOmega were taken on February 2021 positioned immediately around the central field along the stream track. The remaining 11 fields were observed during February and March 2023. Exposure times ranged from 2400 to 8400 s depending on observing and/or weather conditions. The footprint geometry is neither uniform nor symmetric as 2dF failures have prevented us from filling out all the planned fields.

Regarding target selection, we refer the interested reader to Li et al. (2019) for the general S^5 strategy. For Cra2 specifically, astrometric and photometric criteria were adopted. Candidates were vetted to reside within a 0.15 mag color window around a dereddened (Schlegel et al. 1998) empirical isochrone constructed based on known members of MW satellite galaxies (Pace & Li 2019) and shifted to the Cra2 distance modulus (20.35, heliocentric distance of 117.5 kpc; Torrealba et al. 2016) in a *Gaia* (Gaia Collaboration et al. 2016) $G - G_{RP}$

vs. G color–magnitude diagram (CMD; Evans et al. 2018; Riello et al. 2020). Targets were selected to also have proper motions consistent with the mean value for Cra2 (Fritz et al. 2018). Observations taken during 2020 (central fields) used astrometry and photometry from *Gaia* DR2 (Gaia Collaboration et al. 2018), while *Gaia* (early)DR3 (Gaia Collaboration et al. 2021, 2023) was adopted for all others. *Gaia*'s parallaxes were used to remove likely nearby MW contaminants by keeping those targets where `parallax_over_error` < 3. Whenever some of the 392 2dF science fibers were still unused, priority was given to sources with proper motions consistent with Cra2, but outside the $G - G_{RP}$ color window. Within the 14 fields targeted by S^5, a total of 3838 sources were observed out of which 2757 were flagged as stars with good fits by our pipeline (`good_star` = `TRUE` in the S^5 catalog (Li et al. 2019).

Details on the global data processing for S^5 can be found in other collaboration papers (Li et al. 2019, 2021, 2022; Shipp et al. 2021; Koposov et al. 2023). Briefly, we model blue and red arms of AAOmega spectra simultaneously with `RVSpecFit`[25] template fitting code (Koposov 2019, see also Koposov et al. 2011) using a grid of stellar atmospheres and synthetic spectra from the PHOENIX library (Husser et al. 2013) interpolated using a neural network emulator. We also assume a photometric prior on effective temperature with both Dark Energy Camera (DECam; $g-r$ and $r-z$; Flaugher et al. 2015) and *Gaia* ($G - G_{RP}$) colors as in Li et al. (2019). The DECam photometry adopted is from the The DECam Local Volume Exploration Survey (DELVE) DR2 (Drlica-Wagner et al. 2021, 2022). This approach benefits from the wider wavelength coverage in the blue arm (3800–5800 Å), despite lower spectral resolution ($\mathcal{R} \sim 1300$), for better stellar parameter estimates while maintaining good line-of-sight velocity ($v_{\rm hel}$) precision thanks to the higher resolution ($\mathcal{R} \sim$ 10,000) around the calcium triplet (8400–8800 Å) in the red arm.

With the `RVSpecFit` processed data at hand, we perform several quality cuts, in addition to `good_star` = `TRUE`, to ensure the reliability of S^5 DR2 stellar parameters. First, we limit our sample to stars with at least moderate signal-to-noise ratios ($S/N > 3$) in the red arm. The typical $v_{\rm hel}$ uncertainty for RGB stars in S^5 DR2 is $\sim$4 km s^{-1} at this S/N. Then, we remove those stars with very large *Gaia* proper motions in either right ascension (α) or declination (δ) directions: $|\mu_\alpha \cos\delta| > 10$ mas yr^{-1} or $|\mu_\delta| > 10$ mas yr^{-1}. We also convert $v_{\rm hel}$ values to the Galactic standard of rest ($v_{\rm gsr}$) using MW fundamental parameters from `Astropy` (v5.10; Astropy Collaboration et al. 2013, 2018). The distance from the Sun to the Galactic center is 8.122 kpc (Gravity Collaboration et al. 2018), the Sun's velocity vector in the Galactocentric cylindrical frame is $(V_R, V_\phi, V_z)_\odot = (12.9, 245.6, 7.78)$ km s^{-1} (Drimmel & Poggio 2018), and the Sun's vertical displacement with respect to the Galactic plane is 20.8 pc (Bennett & Bovy 2019). We then keep only those stars where $|v_{\rm gsr}| < 500$ km s^{-1}. We also remove stars with large $v_{\rm hel}$ errors of $>$10 km s^{-1}. For stars with large metallicity errors ($>$0.5 dex), we set the [Fe/H] uncertainty to 99 dex, but do not discard them from the sample. This allows us to keep their phase-space information for fitting the Cra2 stream kinematics (Section 3.3), while effectively disregarding them for metallicity determination. These bad velocity and [Fe/H] measurements in S^5 catalog are usually due to issues with sky subtraction, causing large systematic residuals in the spectra. In total, 1100 stars with good-quality velocities are considered for Cra2 membership (Appendix A).

3. METHODS

3.1. *N-body models of Crater 2 and its stellar stream*

For comparison to our new S^5 DR2 data, as well as the Coppi et al. (2024) RRL sample, we compute both cored and cuspy models of Cra2 in the combined potential of the MW and LMC. We evolve these models with a restricted N-body method, which is based on the technique used in Vasiliev et al. (2021). In this approach, we initialize an N-body system with tracer particles and fit these with a low order multipole expansion. We then evolve the tracer particles in this potential until the time for the next potential update. At this moment in time, we recompute the multipole expansion and then evolve the tracer particles in the updated potential. This method has been implemented in `AGAMA` (Vasiliev 2019)[26]. This technique provides a good match to full N-body simulations at a fraction of the computational cost (A. Senkevich et al., in preparation).

For the MW, we use the axisymmetric `MWPotential2014` from Bovy (2015). Following Vasiliev et al. (2021), we model the LMC as a truncated NFW profile (Navarro et al. 1996b, 1997) with a mass of $1.5 \times 10^{11}\, M_\odot$ (Erkal et al. 2019) and a scale radius of $r_s = 10.84$ kpc. This choice of mass and r_s gives a rotation curve at 8.7 kpc consistent with the results from van der Marel & Kallivayalil (2014). As in Vasiliev et al. (2021), we take the

[25] https://github.com/segasai/rvspecfit.

[26] https://github.com/GalacticDynamics-Oxford/Agama/blob/master/py/tutorial_streams.ipynb.

truncation radius to be $10 \times r_s$, equivalent to 108.4 kpc. We include dynamical friction on the LMC by the MW as in Vasiliev et al. (2021). We also account for the reflex motion of the MW in response to the LMC.

For the present-day phase-space coordinates of Cra2, we take heliocentric proper motions from Pace et al. (2022), heliocentric distance from the distance modulus of Torrealba et al. (2016), and systemic $v_{\rm hel}$ from Ji et al. (2021). We note that these choices for both proper motions and $v_{\rm hel}$ are 1σ consistent with the values derived in this work (Section 4.2). For the LMC, we assume proper motions measured from multi-epoch *Hubble Space Telescope* observations (Kallivayalil et al. 2013). For the LMC distance, we utilize the result from the eclipsing-binary measurement by Pietrzyński et al. (2013, 49.97 kpc). The LMC's systemic $v_{\rm hel}$ is from van der Marel et al. (2002, 262 km s^{-1}). We then rewind Cra2 in the combined potential of the MW and LMC for 7 Gyr, at which time it is close to apocenter. We then evolve the system to the present day using the restricted N-body method described above.

We model the stellar component of Cra2 as a Plummer sphere (Plummer 1911) with $r_s = 1.066$ kpc and $M_\star = 3.16 \times 10^5\, M_\odot$ (Ji et al. 2021, and see Equation 5). We include an exponential truncation with a cutoff radius of $10 \times r_s$, i.e., 10.66 kpc, implemented in `AGAMA` using `outerCutoffRadius` = 10.66 kpc. This inclusion eliminates stars at unrealistically large radii. For the cuspy models, we treat the dark matter halo with an NFW profile (Navarro et al. 1996b, 1997). We compute a base realization with total mass $10^{8.6}\, M_\odot$ and fiducial concentration set by the mass–concentration relation of Dutton & Macciò (2014) assuming a Hubble constant of $H_0 = 67.4$ km s^{-1} Mpc^{-1} (Planck Collaboration et al. 2020). We also use an exponential truncation with a truncation radius of two virial radii to eliminate distant dark matter particles. We model the stellar and dark matter components each with 10^6 particles and generate the initial conditions in `AGAMA`. The final velocity dispersion of the dwarf remnant in this model is 5.92 km s^{-1} and we refer to it as `cusp-base`.

In order to find a closer match to the present-day central velocity dispersion of Cra2 without completely destroying the simulated dwarf, we run a grid of alternative simulations with masses between 10^6–$10^9\, M_\odot$ (in steps of 0.2 dex), and with concentrations between 0.1–10 times the expected value from the Dutton & Macciò (2014) relation in steps of 0.333 dex. We find that a cuspy NFW model with mass $10^{7.6} M_\odot$ and fiducial concentration exhibits the lowest present-day dispersion of 3.76 km s^{-1}. Interestingly, this lowest dispersion is still larger than the observed value of $2.34^{+0.42}_{-0.30}$ km s^{-1} measured in Ji et al. (2021) as well as our own findings in this work (see Sections 3.3 and 4.2). We refer to this cuspy model as `cusp-lowmass`.

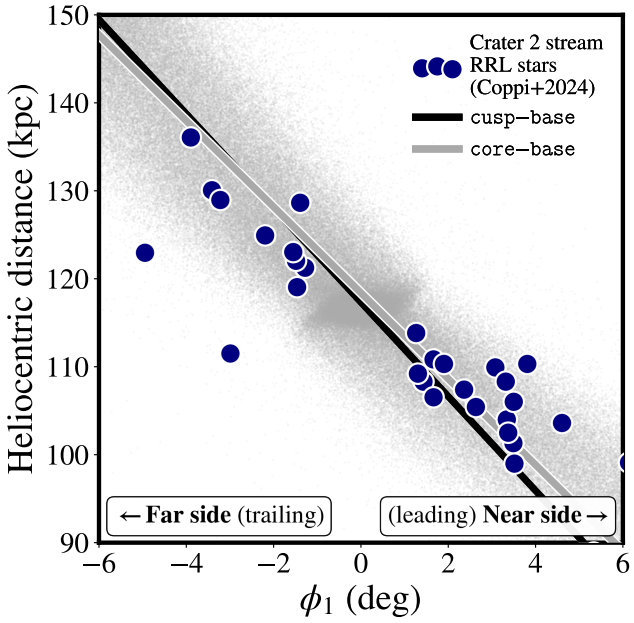

Figure 3. Heliocentric distances as a function of stream longitude ϕ_1 for the Crater 2 (Cra2) system. Dark blue symbols with white edges are RR Lyrae stars associated with the Cra2 stream (Coppi et al. 2024). The simulated Cra2 star particles from the `core-base` model (Section 3.1) are shown as the small gray dots. The gray and black lines represent the -4.9 kpc deg^{-1} and -5.4 kpc deg^{-1} heliocentric distance gradients predicted by the `core-base` and `cusp-base` simulations, respectively.

For the dark matter halos of the cored models, we use the coreNFW prescription from Read et al. (2016). In particular, we consider a maximally cored scenario where the core radius is $1.75 \times r_s$ of our Plummer sphere. As with the cuspy models above, we run a parameter grid with masses in the range 10^7–$10^9\, M_\odot$ (in steps of 0.2 dex) and concentrations between 0.1–10 (in steps of 0.333 dex) times those set by the mass–concentration relation in Dutton & Macciò (2014). We find that a cored model with a mass of $10^{8.6}\, M_\odot$ and a concentration 0.464 times smaller than the fiducial concentration gives the smallest present-day velocity dispersion of 4.79 km s^{-1}. This cored model is dubbed `core-lowc`. We also consider a simulation where the core radius is half the maximally cored value. For this latter cored case, we run a similar grid and find that a mass of $10^{8.6}\, M_\odot$ and a fiducial concentration gives the smallest present-day velocity dispersion of 4.21 km s^{-1}. Given the identical initial mass and concentration to `cusp-base`, we treat this as our `core-base` model. As with the cuspy real-

izations, we generate initial conditions for these dwarfs with `AGAMA` and use 10^6 particles for both stellar and dark matter components. We show a comparison between `cusp-base` and `core-base` models and the Coppi et al. (2024) RRL stars in Figure 3.

From these experiments, we note that the initial mass of the `cusp-lowmass` model is much lower than expected from abundance matching (e.g., Behroozi et al. 2013, 2019; Rodríguez-Puebla et al. 2017), including dwarf-galaxy specific stellar-to-halo mass relations (Garrison-Kimmel et al. 2017; Read et al. 2017; Jethwa et al. 2018; Nadler et al. 2020; Manwadkar & Kravtsov 2022; Danieli et al. 2023; Wang et al. 2024b; Kado-Fong et al. 2025). Hence, we check the cuspy realizations with same initial mass as the best (coldest kinematics) cored simulations, same as `cusp-base` ($10^{8.6}\,M_\odot$), and verify that an NFW halo model with low concentration (0.464 times smaller than the fiducial value, same as the `core-lowc`) produces a central velocity dispersion almost identical ($3.77\,\mathrm{km\,s^{-1}}$) to the `cusp-lowmass` case. We refer to this higher-mass low-concentration cuspy model as `cusp-lowc`. The comparison between our N-body results and the S^5 DR2 Cra2 data is in Section 4.2.

3.2. *Stream coordinates*

Similarly to other stellar stream works where the progenitor is known, we define a convenient coordinate system for our analyses (e.g., Majewski et al. 2003; Li et al. 2018). We define the stream longitude ϕ_1 and latitude ϕ_2 in a way that $(\phi_1, \phi_2) = (0.0, 0.0)$ is located at the on-sky center of Cra2 ($\alpha = 177.310°$ and $\delta = -18.413°$; Torrealba et al. 2016). The Cra2 stream is well aligned with $\phi_2 = 0$. We adopt a position angle of 60° to derive the 3×3 rotation (R) matrix that converts from celestial (α, δ) to stream coordinates (ϕ_1, ϕ_2):

$$\begin{bmatrix} \cos(\phi_1)\cos(\phi_2) \\ \sin(\phi_1)\cos(\phi_2) \\ \sin(\phi_2) \end{bmatrix} = R \times \begin{bmatrix} \cos(\alpha)\cos(\delta) \\ \sin(\alpha)\cos(\delta) \\ \sin(\delta) \end{bmatrix}. \quad (1)$$

The rotation matrix entries R_{ij} are presented to a precision of 8 significant digits,

$$\begin{aligned} R &= \begin{bmatrix} R_{00} & R_{01} & R_{02} \\ R_{10} & R_{11} & R_{12} \\ R_{20} & R_{21} & R_{22} \end{bmatrix} \\ &= \begin{bmatrix} -0.94775886 & 0.04452939 & -0.31586432 \\ -0.19840253 & -0.85765902 & 0.47440218 \\ -0.24977905 & 0.51228716 & 0.82168869 \end{bmatrix}, \end{aligned} \quad (2)$$

and aligns well with the Coppi et al. (2024) RRL stars. See Koposov et al. (2010) and Shipp et al. (2019) for a similar formalism applied to other stellar streams.

3.3. *Stellar kinematics and membership*

To identify Cra2 members across the entire S^5 footprint, we model the galaxy's remnant body and stream kinematics in a Bayesian mixture modeling framework. This probabilistic approach has already been extensively employed to disentangle members of stellar streams, as well as dwarf galaxies and globular clusters, from their surrounding back/foreground (Martin et al. 2008; Walker et al. 2009, 2016; Li et al. 2018; Pace & Li 2019; Pace et al. 2022), including S^5 works (Shipp et al. 2019; Li et al. 2022; Awad et al. 2025). We model the distributions of *Gaia* proper motions, including correlations between $\mu_\alpha \cos\delta$ and μ_δ, and `RVSpecFit` $v_{\rm hel}$ and [Fe/H] within S^5 DR2 Cra2 fields with three components. One of these corresponds to the actual Cra2 system, including galaxy and stream. The other two components represent the foreground contamination from the MW's disk and halo. For an unbiased identification of Cra2 members in its outskirts and stream, we do not consider spatial priors.

We model $v_{\rm gsr}$, [Fe/H], and proper motions as Gaussian distributions for both Cra2 (galaxy plus stream) and foreground components. The full likelihood functions are written elsewhere (Walker et al. 2009, 2016; Li et al. 2018; Pace & Li 2019; Awad et al. 2025). Following the expectation from the stream N-body models (Section 3.1), we adopt a linear dependence of mean $v_{\rm gsr}$ with ϕ_1 in the form

$$v_{\rm gsr}(\phi_1) = \left(\frac{\Delta v_{\rm gsr}}{\Delta\phi_1}\right)\phi_1 + v_{\rm gsr}(\phi_1 = 0), \quad (3)$$

where $\Delta v_{\rm gsr}/\Delta\phi_1$ is the velocity gradient and $v_{\rm gsr}(\phi_1 = 0)$ is Cra2's mean systemic $v_{\rm gsr}$ at $\phi_1 = 0$. We found a significant velocity gradient at the $\approx 7\sigma$ level:

$$\frac{v_{\rm gsr}(\phi_1)}{\mathrm{km\,s^{-1}}} = \frac{(-4.5 \pm 0.6)}{\mathrm{deg}}\phi_1 + (-81.2 \pm 0.3), \quad (4)$$

where this systemic $v_{\rm gsr}$ is compatible (1σ) with previous results (Caldwell et al. 2017; Fu et al. 2019; Ji et al. 2021). Implications and comparisons with the N-body models are in Section 4.2.

For metallicity, we assume a linear radial gradient with $|\phi_1|$. We have explored using a quadratic function instead, which might be appropriate for some dwarf galaxies (see Taibi et al. 2022). However, we found no evidence for a significant [Fe/H] gradient in either case. The mean central metallicity ($\langle$[Fe/H]$\rangle = -2.16 \pm 0.04$) and dispersion ($\sigma_{\rm [Fe/H]} = 0.28 \pm 0.03$) we found are effectively identical to the values from Ji et al. (2021). We also assume a linear dependence with ϕ_1 for the proper motions, but found no significant evidence for variations. The mean systemic proper motions we found

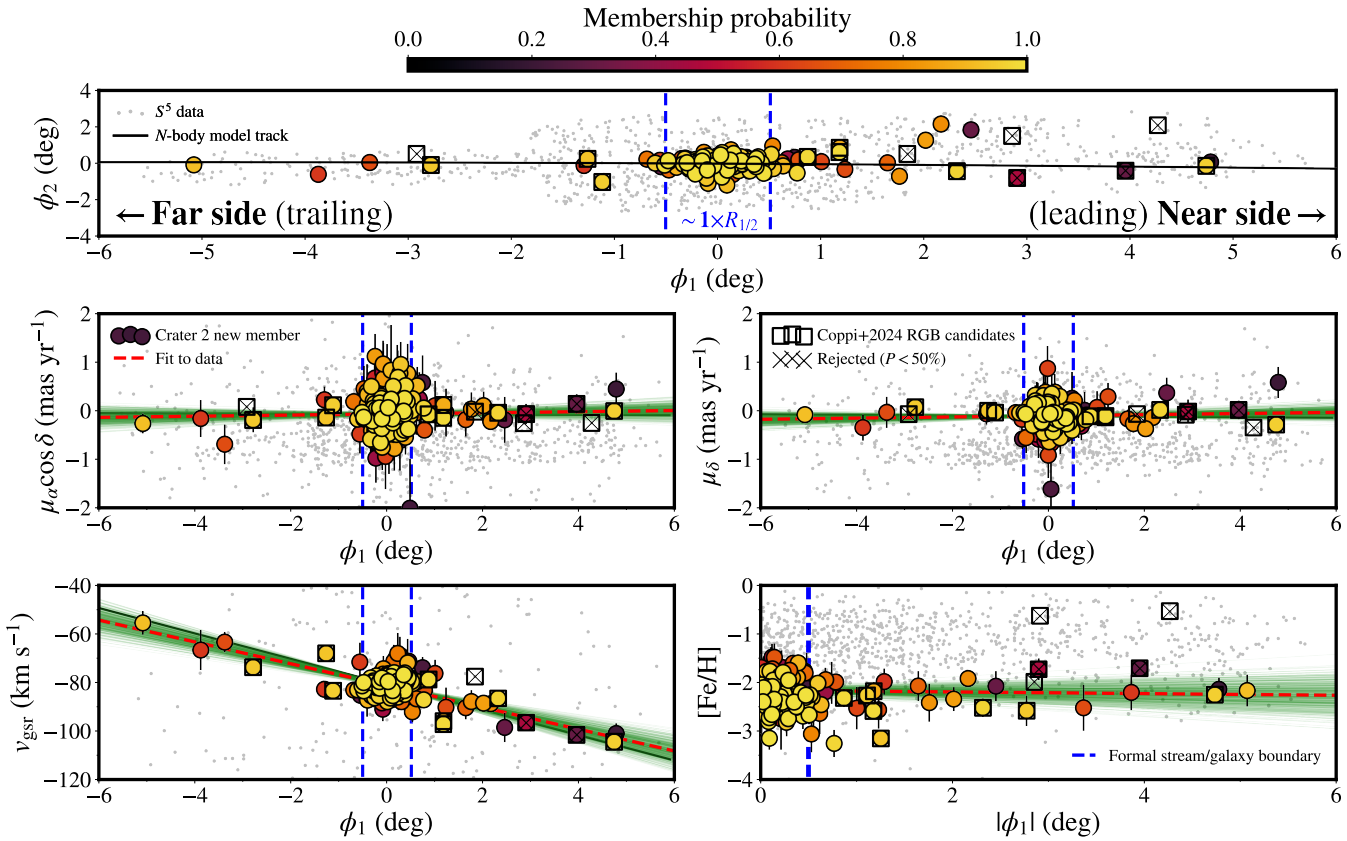

Figure 4. Mixture modeling fit results. Top panel: Crater 2 (Cra2) stream coordinates (ϕ_1, ϕ_2) distribution (Section 3.2). The far (trailing arm) and near (leading) sides of the stream are annotated. Middle: linear proper motion gradients as a function of stream longitude ϕ_1. Bottom left: linear Galactic standard of rest line-of-sight velocity ($v_{\rm gsr}$) gradient. Bottom right: radial metallicity ([Fe/H]) gradient. In all panels, Cra2 candidates ($P > 20\%$) in the S^5 DR2 footprint are color-coded by their membership probabilities. Non-members that have also been observed by S^5 are plotted as gray dots. Red dashed lines represent the mean values from our best-fit mixture model while the thin green lines show 200 realizations of our fit sampled from our posterior chains. The black solid lines are linear fits to our `core-base` simulated stream track (Section 3.1). Red giant-branch Cra2 stream candidates from Coppi et al. (2024) are plotted as black open squares. Those with available S^5 DR2 data, but rejected as true members, are displayed as black 'X' symbols. In all panels, blue dashed lines delineate the formal boundary between galaxy and stream in our mixture modeling analysis (Section 3.3).

are, again, 1σ consistent with other works (Fritz et al. 2018; Ji et al. 2021; Battaglia et al. 2022; Pace et al. 2022); $\langle \mu_\alpha \cos\delta \rangle = -0.070 \pm 0.020\,{\rm mas\,yr^{-1}}$ and $\langle \mu_\delta \rangle = -0.107 \pm 0.013\,{\rm mas\,yr^{-1}}$. For the foreground components, we assume no spatial dependence for any of these parameters.

To account for Cra2's galaxy and stream kinematics separately, we assume that the fraction of members in the sample changes depending on ϕ_1 (similar to Awad et al. 2025). Formally, our model incorporates a "central fraction" and a "stream fraction" terms which are defined inside and outside the boundary $|\phi_1| = 0.5°$ (∼Cra2's $R_{1/2}$; Torrealba et al. 2016). This inclusion is necessary since adopting a single fraction for the whole galaxy would artificially increase the membership probability (P) of stars in the stream while decreasing it for Cra2's central region. This stream–galaxy boundary also serves for us to estimate the velocity dispersion in the stream and remnant body separately. For the central velocity dispersion of Cra2, we found $\sigma_{v,\rm gal} = 2.51^{+0.33}_{-0.30}$ km s^{-1}. For the stream, we obtained $\sigma_{v,\rm str} = 5.74^{+0.98}_{-0.83}$.

We sample posterior distributions with a Markov chain Monte Carlo approach using the `emcee` package (Foreman-Mackey et al. 2013) with 200 walkers and 20,000 steps, including a burn-in stage of 10,000. We take 16$^{\rm th}$ and 84$^{\rm th}$ percentiles as uncertainties for all parameters, including the ones already listed in the previous paragraphs. The model fitting results are mostly presented in Figure 4 where Cra2 candidate stars at $P > 20\%$ are color-coded by their individual membership probability values. We present the full quantitative results in Section 4.

Table 1. Crater 2 galaxy properties

Parameter	Value	Unit	Source	Description
α	177.310	deg	Torrealba et al. (2016)	Center right ascension
δ	−18.413	deg	Torrealba et al. (2016)	Center declination
$m-M$	20.35±0.02	[mag]	Torrealba et al. (2016)	Distance modulus
$d_{\rm hel}$	117.5±1.1	kpc	Torrealba et al. (2016)	Heliocentric distance
M_V	−8.2	[mag]	Torrealba et al. (2016)	V-band absolute magnitude
$R_{1/2}$	1054^{+93}_{-89}	pc	Pace (2025)[a]	Physical circularized half-light radius
$R_{1/2}$	31.2 ± 2.5	arcmin	Torrealba et al. (2016)	Projected angular half-light radius
ϵ	<0.1[b]		Torrealba et al. (2016)	Ellipticity
μ_V	30.5	[mag]	Pace (2025)[a]	Average surface brightness within $R_{1/2}$
$M_\star$	$10^{5.5}$	$M_\odot$	Equation 5	Stellar mass[c]
$\mu_\alpha \cos\delta$	−0.070±0.020	mas yr^{-1}	This work	Heliocentric proper motion (α)
μ_δ	−0.107±0.013	mas yr^{-1}	This work	Heliocentric proper motion (δ)
$v_{\rm hel}$	$+89.2 \pm 0.3$	km s^{-1}	This work	Heliocentric line-of-sight velocity
$v_{\rm gsr}$	-81.2 ± 0.3	km s^{-1}	This work	Galactic standard of rest line-of-sight velocity
$\sigma_{v,\rm gal}$	$2.51^{+0.33}_{-0.30}$	km s^{-1}	This work	Line-of-sight velocity dispersion within $R_{1/2}$
$\sigma_{v,\rm str}$	$5.74^{+0.98}_{-0.83}$	km s^{-1}	This work	Line-of-sight stream velocity dispersion
$\sigma_{v,\rm str}/\sigma_{v,\rm gal}$	$2.30^{+0.41}_{-0.35}$		This work	Velocity dispersion ratio between stream and galaxy
$\Delta v_{\rm gsr}/\Delta\phi_1$	-4.5 ± 0.6	km s^{-1} deg^{-1}	This work	$v_{\rm gsr}$ gradient as a function of stream longitude ϕ_1
$\langle$[Fe/H]$\rangle$	-2.16 ± 0.04	[dex]	This work	Mean central metallicity
$\sigma_{\rm [Fe/H]}$	0.28 ± 0.03	[dex]	This work	Metallicity dispersion
$\Delta d_{\rm hel}/\Delta\phi_1$	−4.9	kpc deg^{-1}	This work	N-body model $d_{\rm hel}$ gradient with ϕ_1[d]
$r_{\rm apo}$	154.31	kpc	This work	N-body model orbital apocenter
$r_{\rm peri}$	22.26	kpc	This work	N-body model orbital pericenter
e	0.75		$e = \frac{r_{\rm apo} - r_{\rm peri}}{r_{\rm apo} + r_{\rm peri}}$	N-body model orbital eccentricity

[a]Local Volume Database with structural parameters from Torrealba et al. (2016).
[b]Upper limit at 95% confidence level. We adopt $\epsilon = 0.0$ in Figures 1 and 2.
[c]Assuming mass-to-light ratio $\eta = 2$ and the Sun's absolute V-band magnitude $M_{V,\odot} = +4.81$.
[d]Average between all N-body models considered (Section 3.1).

Out of the 1100 stars with good `RVSpecFit` parameters in the S^5 DR2 catalog within the footprint that pass all quality criteria (Section 2), we identify 143 Cra2 members ($P > 50\%$) out of which 114 belong to the main body of the galaxy (within its $R_{1/2}$; Torrealba et al. 2016; Vivas et al. 2020) and 29 are associated with the stellar stream. From these numbers, we can naively estimate a lower limit for Cra2's $M_\star$ loss of $21 \pm 7\%$ (Wilson score interval at 95% confidence level; Wilson 1927). Cra2 star members in the S^5 footprint can be found out to $\gtrsim$10× its on-sky angular $R_{1/2}$ (>20 kpc physical separation), aligned in a stream-like morphology that matches the expected debris track (Figure 2). Note that we observe Cra2 stars across the entire S^5 coverage and, therefore, are yet to reach the edge of the stellar stream. Our mixture modeling results, as well as other Cra2 galaxy properties, are listed in Table 1.

4. RESULTS

The most obvious takeaway from our analysis of S^5 DR2 data is the unequivocal detection of a stellar stream attached to the Cra2 dwarf galaxy remnant and, therefore, that this system is experiencing severe tidal disruption. Below, we list other results alongside pertinent discussions.

4.1. *Discovery of red giant-branch stars in the Crater 2 stream*

In comparison to previous S^5 work (Ji et al. 2021), we recover almost all members within Cra2's central region. The few stars that were considered members by Ji et al. (2021), but are now attributed $P < 50\%$, are usually the most metal-rich ones in the sample at [Fe/H] $\gtrsim -1.5$. Out of our 143 members, 114 are located within $|\phi_1| < 0.5°$ (∼Cra2's $R_{1/2}$). The remaining 29 stars are formally members of the stream in our mixture model. The farthest Cra2 stream star within the

S^5 DR2 footprint is found at $\sim$10$\times$ Cra2's on-sky $R_{1/2}$ and $\gtrsim$20 kpc physical separation given the expected distance gradient. As can be appreciated from Figure 5, the majority of the new Cra2 RGB members are contained within very metal-poor ([Fe/H] = −2.0 and −2.5) Dartmouth isochrones (Dotter et al. 2008) of old stellar populations (12.5 Gyr, [α/Fe] = +0.4) in a DECam $g-r$ vs. absolute r-band magnitude (M_r) CMD (DELVE DR2 photometry; Drlica-Wagner et al. 2022). Absolute magnitudes for our sample are computed assuming the heliocentric distance predicted for Cra2 tidal tails from our `core-base` stream model (Figure 3). The narrow color range covered by Cra2's RGB is in line with the deep CMD analysis by Walker et al. (2019).

A total of 24 potential RGB members were identified in the Cra2 stream by Coppi et al. (2024). Out of these, 14 are located within the S^5 DR2 footprint and were observed as part of the program (square symbols in Figure 2). We confirm that 8 of these RGB stars are, indeed, associated with the Cra2 stream with high probability, all at $P \geq 88\%$ (Table 2). All these new Cra2 stream stars exhibit very low metallicities ($-3.2 \lesssim$ [Fe/H] < -2.2) and $v_{\rm gsr}$ values consistent with the predicted `core-base` stream track (bottom left panel of Figure 4). Some of the other candidates are rejected due to their discrepant $v_{\rm gsr}$ (CS4, WS2, and WS5; $P = 0.0$ in Table 2), which are even outside the plot boundaries in the ϕ_1 vs. $v_{\rm gsr}$ panel in Figure 4. Star CS12 is $\sim$20 km s^{-1} displaced from the fitted $v_{\rm gsr}(\phi_1)$ track at the same time that it has a very high metallicity, though also quite uncertain, in the S^5 DR2 catalog ([Fe/H] $\approx +0.4 \pm 0.5$). The rest of the Coppi et al. (2024) candidates (CS13, and WS4) are attributed $30\% \leq P < 50\%$ likely due to their relatively high metallicities ([Fe/H] ≈ -1.7).

Despite the above-described overall success of Coppi et al.'s (2024) method for finding Cra2 stream members, there was still some contamination. We verify that all the rejected candidates from these authors' sample turned out to be those redder, in DECam $g-r$ color, than most of the Cra2 members found in S^5 DR2. In the DECam $g-r$ vs. M_r CMD shown in Figure 5, the rejected Cra2 RGB candidates are all redder than expected from the [Fe/H] = −2 Dartmouth isochrone, some being redder than the [Fe/H] = −1.5 track. The S^5 spectroscopically vetted members are almost entirely confined within, or bluer than, the [Fe/H] = −2.0 and −2.5 isochrones. Hence, narrowing the color window around Cra2's RGB sequence and adding information regarding the predicted distance gradient might be advantageous when searching for additional stream members even farther away from this galaxy's center.

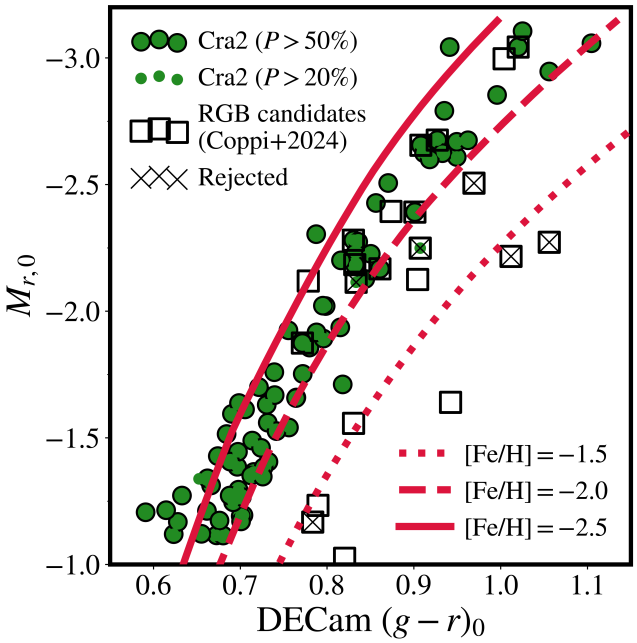

Figure 5. Dereddened DECam $(g-r)_0$ vs. $M_{r,0}$ color–magnitude diagram covering the red giant branch (RGB) with photometry from DELVE DR2 (Drlica-Wagner et al. 2022) for stars in the S^5 DR2 footprint with Crater 2 (Cra2) membership probability $P > 50\%$ (green circles with black edges) and $20\% < P \leq 50\%$ (green dots). The absolute r-band magnitude is computed assuming the expected distance gradient from our Cra2 `core-base` model (Section 3.1). The Coppi et al. (2024) Cra2 RGB candidates are plotted as the open squares, with the rejected ones having an 'X' symbol on top. Red lines are (12.5 Gyr, [α/Fe] = +0.4) Dartmouth isochrones (Dotter et al. 2008) with [Fe/H] = −2.5 (solid), −2.0 (dashed), and −1.5 (dotted).

4.2. *Kinematics along the Crater 2 stellar stream and insights on its dark matter content*

An important immediate byproduct of our kinematic analysis is our $\approx 7\sigma$ detection and determination of a velocity gradient across the Cra2 system; $\Delta v_{\rm gsr}/\Delta\phi_1 = (-4.5 \pm 0.6)$ km s^{-1} deg^{-1}. This quantity can be used as an additional constraint to future tailored simulations of Cra2 trying to reproduce its structural properties. A comparison between S^5 DR2 new Cra2 RGB members and the stream `core-base` model track, alongside our linear fit to the $v_{\rm gsr}$ gradient, is presented in the bottom left panel of Figure 4. The output $v_{\rm gsr}(\phi_1)$ values from our N-body simulations are in reasonable agreement with observations within the on-sky coverage of S^5 DR2, the range of model velocity gradients being within −4.6 and −5.4 km s^{-1} deg^{-1}.

In dark matter-only tidal disruption simulations, Errani et al. (2015) showed that the velocity-dispersion ratio between stream and central region in a dwarf galaxy

Table 2. Crater 2 stream red giant-branch candidates from Coppi et al. (2024) with S^5 DR2 observations

Gaia DR3 `source_id`	Name (Coppi et al. 2024)	α (deg)	δ (deg)	$g^\dagger$	$r^\dagger$	$v_{\rm hel}$ ($\rm km\,s^{-1}$)	$v_{\rm gsr}$ ($\rm km\,s^{-1}$)	[Fe/H]	P
3546585982161428736	CS4	174.3575	−19.3930	19.3	18.2	2.6±1.3	−175.7	−0.64±0.10	0.00
3542009329433731072	CS5	174.7955	−19.8505	19.7	18.8	104.7±3.6	−73.8	−2.59±0.32	0.94
3543686119025619200	CS6	176.0250	−18.8178	18.8	17.8	105.8±1.2	−68.1	−3.16±0.11	0.93
3542608597631389568	CS7	176.8130	−19.8322	18.8	17.8	91.3±1.0	−83.4	−2.27±0.10	0.96
3544050091734226304	CS8	177.9139	−17.6618	18.9	18.0	88.7±1.2	−78.8.1	−2.33±0.18	0.98
3567352213460408960	CS9	179.6337	−17.5965	18.9	18.1	77.4±1.3	−86.5	−2.52±0.19	0.97
3568269210454897792	CS10	178.0557	−17.2831	18.4	17.3	69.2±0.9	−97.1	−2.59±0.07	0.98
3568288486268051712	CS11	177.9339	−17.0760	18.9	18.1	70.2±1.3	−95.9	−2.19±0.19	0.88
3568206877592789888	CS12	178.7070	−17.0423	19.2	18.1	86.9±1.2	−77.6	+0.42±0.53	0.19
3567764324162907520	CS13	181.0822	−16.7292	18.9	18.0	57.4±1.3	−101.5	−1.72±0.17	0.30
3567951176715579008	CS14	181.6388	−16.1012	18.8	17.9	51.8±1.1	−104.4	−2.26±0.16	0.96
3568907335219100032	WS2	179.0963	−15.6769	19.9	19.0	266.8±2.0	+106.4	−1.99±0.19	0.00
3567316960369373696	WS4	180.3542	−17.6119	18.9	18.0	66.0±2.3	−96.5	−1.73±0.23	0.46
3570603950380122496	WS5	180.0465	−14.4625	18.9	17.8	127.7±1.7	−27.6	−0.54±0.15	0.00

†DECam g and r photometry reported in DELVE DR2 (Drlica-Wagner et al. 2022).

($\sigma_{v,\rm str}/\sigma_{v,\rm gal}$) is sensitive to its dark matter density profile. In general, disrupted cored dark matter halos will exhibit higher values of $\sigma_{v,\rm str}/\sigma_{v,\rm gal}$ than cuspy ones. The reason for that is because, to reproduce a fixed value of central velocity dispersion ($\sigma_{v,\rm gal}$), cored halos require a larger total mass than cuspy ones. As a result, the tidal radii, i.e., the sizes, of cored dark matter halos are larger than cuspy ones, leading to dynamically hotter and spatially wider tidal streams. Furthermore, dwarf galaxies embedded in cored dark matter halos cool down more efficiently during tidal stripping than their cuspy counterparts, leading to increasing $\sigma_{v,\rm str}/\sigma_{v,\rm gal}$ over time. Note that hydrodynamical simulations predict that most dwarf satellites around MW-like hosts should be tidally disrupting, but their associated stellar streams would have surface brightnesses that are too faint to be detected in current photometric data (Shipp et al. 2023, 2025; Riley et al. 2025). Therefore, future kinematic studies of yet-undiscovered stellar streams around seemingly unscathed MW satellites might be crucial for inferring their true dark matter mass profiles.

According to the Errani et al. (2015) calculations for a dwarf galaxy on an orbit of similar eccentricity to Cra2 ($e \sim 0.7$; Fu et al. 2019; Ji et al. 2021; Pace et al. 2022), an NFW cuspy halo would produce $\sigma_{v,\rm str}/\sigma_{v,\rm gal} \leq 1$ while the cored case gives $\sigma_{v,\rm str}/\sigma_{v,\rm gal} \gtrsim 3$. The ratio we estimate from the S^5 DR2 Cra2 data is $\sigma_{v,\rm str}/\sigma_{v,\rm gal} = 2.30^{+0.41}_{-0.35}$. At face value, this result disfavors an NFW cuspy halo, thus supporting the hypothesis of a dark matter core in Cra2. We also fit σ_v values for both Cra2 stream and remnant separately with only high-probability members ($P > 50\%$) and found an almost identical ratio of $\sigma_{v,\rm str}/\sigma_{v,\rm gal} = 2.41^{+0.81}_{-0.64}$, confirming the robustness of this measurement.

Unfortunately, the direct comparison of the Errani et al. (2015) models to the S^5 data has several limitations. For instance, these authors' simulations do not account for the infalling LMC system. Additionally, Cra2's remnant body itself might not be in equilibrium. After an impulsive perturbation, such as a pericentric passage around the MW, a dwarf galaxy might undergo a damped-oscillation phase with short-period velocity dispersion variations that could affect the $\sigma_{v,\rm str}/\sigma_{v,\rm gal}$ measurement (Errani et al. 2025). It is also unclear how the galaxy's self-gravity might affect the stream kinematics close to the progenitor. Moreover, Errani et al. (2015) focuses on the velocity dispersion perpendicular to the stream plane, whereas S^5 velocities are line-of-sight measurements, which, despite accounting for the on-sky $v_{\rm hel}$ gradient in our mixture modeling, might still contain projection effects of both the in-plane and perpendicular motions. Perhaps the most critical caveat is that the Errani et al. (2015) predictions for stream kinematics were taken a lot farther away from their simulated dwarf galaxies' centers (from 20 to 100 kpc) than the S^5 DR2 coverage for Cra2.

Here, we test if our own tailored cuspy and cored N-body models (Section 3.1) can reproduce the kinematics of Cra2's stream and galaxy. Although they do not exactly reproduce the present-day phase-space properties of the Cra2 system (e.g., central velocity dispersion), these models should provide qualitative insights

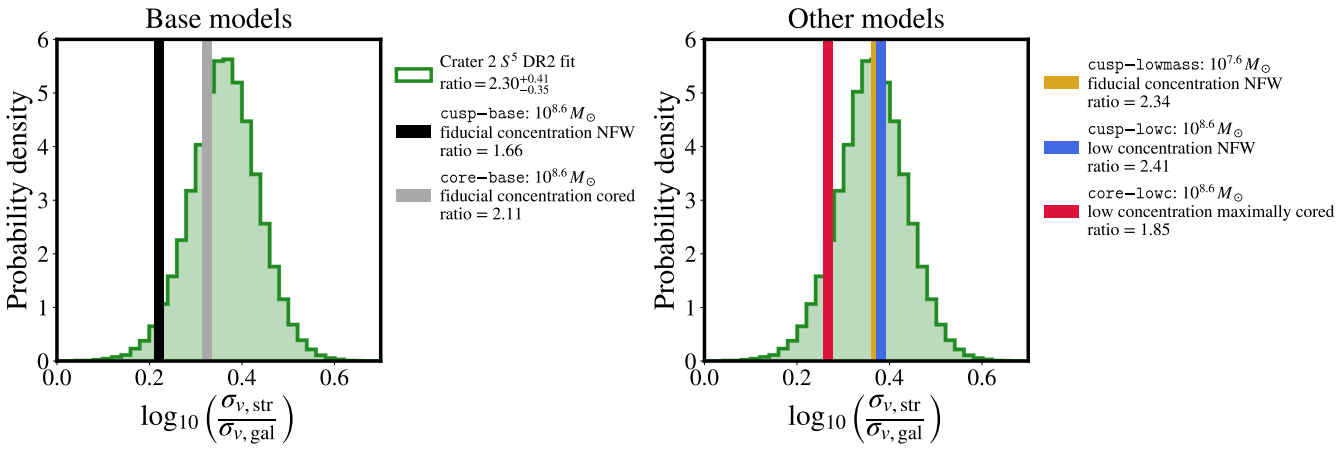

Figure 6. Distribution of velocity dispersion ratio between Cra2 stellar stream and remnant galaxy ($\sigma_{v,\mathrm{str}}/\sigma_{v,\mathrm{gal}}$) in logarithmic scale sampled from our mixture modeling results applied to the S^5 DR2 data (green histograms). Vertical lines represent the results for the velocity dispersion ratio of the different N-body models described in Section 3.1 using a similar method as for the S^5 data. Left panel shows the comparison with the base models ($10^{8.6}\,M_\odot$ halo mass, fiducial concentration), namely `cusp-base` (NFW cuspy, black line) and `core-base` (cored, gray). Right panel shows the alternative models (see text for details): `cusp-lowmass` ($10^{7.6}\,M_\odot$, fiducial concentration NFW, yellow), `cusp-lowc` ($10^{8.6}\,M_\odot$, low concentration NFW, blue), and `core-lowc` ($10^{8.6}\,M_\odot$, low concentration maximally cored, red).

on their behavior. In this vein, our N-body experiments show that halo concentration has an effect on the system's final kinematics degenerate with initial mass. The `cusp-lowmass` ($10^{7.6}\,M_\odot$, fiducial concentration; Dutton & Macciò 2014) and `cusp-lowc` ($10^{8.6}\,M_\odot$, lower concentration) models reached identical central velocity dispersions despite the latter being 10× more massive, echoing results by Amorisco (2019).

In our suite of N-body simulations, the limiting factor on how dynamically cold the model dwarfs can be is the complete disruption of satellites if halo mass and/or concentration are too low. For the cored halo case, however, not only halo mass and concentration are relevant, but the core radius also plays a role. The remnant velocity dispersion of the `core-lowc` model (maximally cored scenario; Read et al. 2016) is larger than in the `core-base` model (half the core radius value) despite the lower concentration of the former.

To quantitatively compare Cra2's observed kinematics to the simulation results, we fit line-of-sight velocities as Gaussian distributions for both galaxy and stream in all N-body models with `emcee` (Foreman-Mackey et al. 2013) accounting for spatial gradients (results in Figure 6). This method is analogous to that applied to the S^5 DR2 data (Section 3.3), but without the need for MW foreground components. The `cusp-lowmass`, `cusp-lowc`, and `core-base` models can all reproduce (1σ) the velocity dispersion ratio between Cra2 stream and remnant body measured from S^5 DR2 data (see text above). The `cusp-base` and `core-lowc` models show lower ratio values, but still within $\lesssim 2.0\sigma$ and 1.5σ, respectively. We recall that the `cusp-lowmass` model has an unrealistically low initial mass compared to abundance matching expectations in the dwarf-galaxy regime (e.g., Garrison-Kimmel et al. 2017; Jethwa et al. 2018; Nadler et al. 2020; Manwadkar & Kravtsov 2022; Danieli et al. 2023; Kado-Fong et al. 2025). Hence, similar to previous works, we judge that an NFW halo progenitor with fiducial concentration is unlikely for Cra2. Although a much broader exploration with N-body simulations will be required to obtain robust conclusions, we find that both cuspy profiles with low concentration and cored halos with small core radius are promising directions to explain Cra2's unique properties.

4.3. *Crater 2 is metal-poor compared to the Local Group stellar mass–metallicity relation*

Another byproduct of our mixture modeling is the determination of the mean metallicity of Cra2 to be $\langle[\mathrm{Fe/H}]\rangle = -2.16 \pm 0.04$ (full metallicity distribution in left panel of Figure 7), adding to the census of Local Group dwarf galaxies with chemical information. With the current data, we find no evidence for [Fe/H] variations as function of ϕ_1 across the Cra2 system (bottom right panel of Figure 4). Metallicity gradients are commonly found in Local Group dSph galaxies (e.g., Taibi et al. 2022), including distinguishable chemo-dynamical populations (Pace et al. 2020; Arroyo-Polonio et al. 2024). However, the latter usually requires metallicities for >1000 stars in a given dSph, while we only identify 143 Cra2 members (at $P > 50\%$) in the S^5 DR2 footprint. Given the large on-sky extent of Cra2, a plausible strategy to test for the presence of spatial [Fe/H] changes

might be to use wide-field photometric metallicities (as in Barbosa et al. 2025 for Sculptor dSph).

We now compare Cra2's mean metallicity derived from S^5 DR2 data to the demographics of Local Group dwarfs by placing this galaxy in the MZR of Kirby et al. (2013, also Simon 2019). For consistency, most metallicity information for the sample of dwarf galaxies in the right panel of Figure 7 is either from Kirby et al. (2013) or Simon (2019). The only exceptions are the LMC and SMC for which average [Fe/H] values were obtained based on the members from Nidever et al. (2020) with updated data from the Apache Point Observatory Galactic Evolution Experiment (APOGEE; Majewski et al. 2017; Abdurro'uf et al. 2022, DR17) by Limberg et al. (2022). All the M_V values are from the Pace (2025) compilation. We homogeneously compute corresponding $M_\star$ for the displayed M_V interval:

$$\frac{M_\star}{M_\odot} = \eta 10^{0.4(M_{V,\odot}-M_V)}, \tag{5}$$

where $\eta = 2$ is the assumed mass-to-light ratio and $M_{V,\odot} = +4.81$ (Willmer 2018). Average metallicities for other diffuse dwarfs Ant2 and And19 are from Ji et al. (2021, $\langle$[Fe/H]$\rangle = -1.90$) and Collins et al. (2020, -2.07), respectively.

Arguably, the most intriguing observational fact about the collective of diffuse dwarfs in the Local Group is that they are all metal-poor compared to the expectation from the Local Group MZR for their luminosity (Kirby et al. 2013; Simon 2019). Ant2, Cra2, and And19 are located $\sim$1.0, 1.5, and 2.0σ, respectively, below the MZR assuming the root mean square scatter of 0.16 dex around $\langle$[Fe/H]$\rangle$ derived by Kirby et al. (2013). We note that, despite both slope and intercept of the linear relation from Simon (2019) being identical to Kirby et al.'s (2013), the scatter found by the former is inflated due to the presence of ultra-faint dwarf (UFD) galaxies ($M_\star \lesssim 10^5\,M_\odot$) in their fit, so we consider the latter. Although the diffuse dwarfs do not individually represent major deviations from the MZR, it is certainly unusual that all of them have lower-than-expected metallicities, hinting at a shared formation/evolution channel.

The location of diffuse dwarf galaxies relative to the Local Group MZR becomes more noteworthy since we are now positive that at least Cra2 is experiencing severe tidal disruption. When a galaxy loses stellar content, it should end up appearing metal-*rich* compared to the MZR (Riley et al. 2025); such is the case for Sagittarius dSph (e.g., Hayes et al. 2020, see "Sgr" annotation in the right panel of Figure 7). Also, the Sagittarius dSph has experienced preferential stripping of its low-[Fe/H] population (Limberg et al. 2023; Cunningham et al. 2024), which further contributes to its displacement from the MZR[27] (Riley et al. 2025). Contrary to Sagittarius dSph, Cra2 is metal-*poor* relative to the MZR and accounting for $M_\star$ loss exacerbates such discrepancy. Previous works have argued that, to reproduce the large $R_{1/2}$ and small σ_v of Cra2 in an NFW dark matter halo, it would require >90% loss of stellar content through tides (e.g., Fattahi et al. 2018; Applebaum et al. 2021). Compensating for 90% (99%) $M_\star$ loss results in an M_V difference of 2.5 (5.0) mag, which would bring the tension with the MZR to the 3σ (5σ) level (white '$\star$' symbols with green edges in Figure 7).

In the spirit of the above discussion, the fact that And19 is metal-poor relative to the Local Group MZR was actually used as an argument against the tidal disruption mechanism to explain this galaxy's large size by Collins et al. (2022, but see results by Cullinane et al. 2024). Confirming And19's orbit around M31 with direct proper-motion measurements will be crucial to confirm (or falsify) that this galaxy is not experiencing mass loss through tides. However, given the counter-example of Cra2, we can now assert that low metallicity and tidal disruption are not mutually exclusive.

There is evidence that Ant2 is also being tidally disrupted (Ji et al. 2021), but its deviation from the MZR is less extreme than Cra2's and And19's (see Figure 7). In fact, Riley et al. (2025) has recently argued based on hydrodynamical galaxy-formation simulations that up to $\sim$80% $M_\star$ loss is still plausible for a displacement from the MZR similar to that observed in Cra2 and Ant2, but more than that, as required in the case of a cuspy NFW halo (Fattahi et al. 2018; Applebaum et al. 2021), is difficult to explain. Indeed, one way to alleviate this tension between the diffuse dwarfs and the MZR might come from the evidence for either a cored density profile or a low-concentration NFW halo; for a fixed enlargement factor, these models require less total mass loss than cuspy ones with fiducial concentration (Errani et al. 2015; Amorisco 2019; Fu et al. 2019).

5. DISCUSSION

Collins et al. (2022) discussed possible formation mechanisms for the unusual properties of And19, which are all in common with Cra2: (*i*) the colossal size for its $M_\star$, hence extremely low surface brightness (Torrealba et al. 2016), (*ii*) minuscule central velocity dispersion (Caldwell et al. 2017; Fu et al. 2019), (*iii*) lower-than-expected metallicity in comparison to the Local Group

[27] With APOGEE DR17, the mean metallicities of Sagittarius dSph remnant galaxy and stream are $\langle$[Fe/H]$\rangle = -0.58$ and -1.07, respectively (Hayes et al. 2020; Limberg et al. 2022)

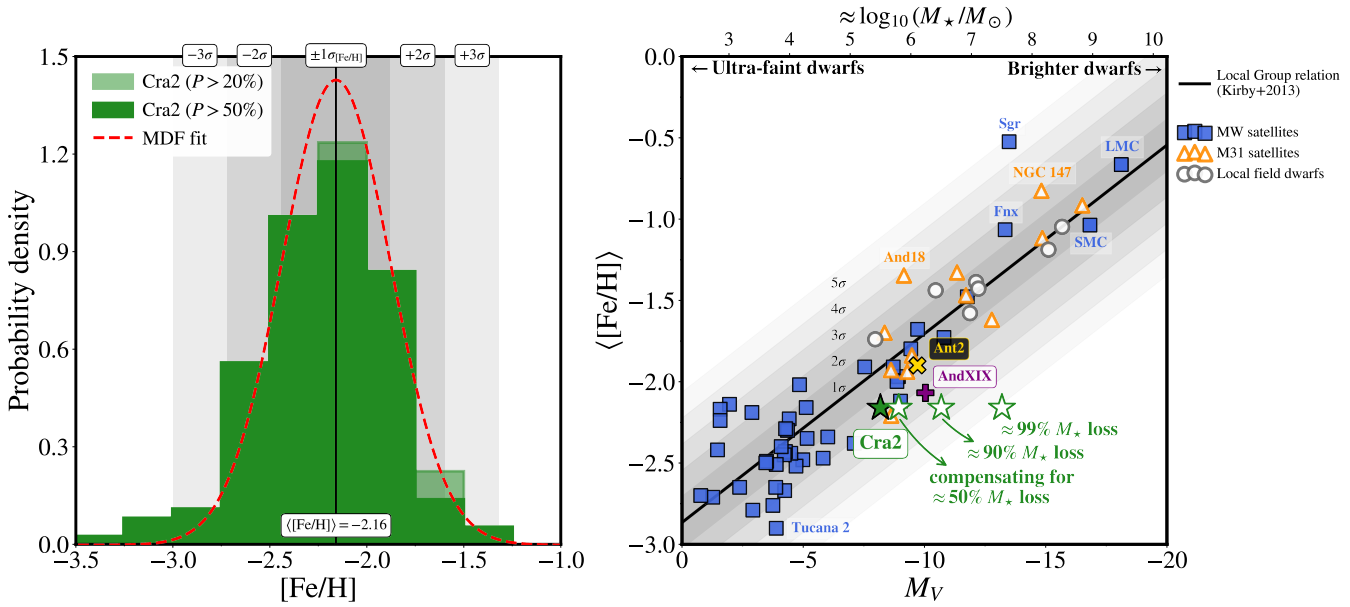

Figure 7. Left: Crater 2 (Cra2) metallicity distribution function (MDF) for membership probability $P > 50\%$ stars (green histogram). The transparent green histogram shows the same, but for $P > 20\%$. The binning is set to 0.25 dex, which is compatible with the S^5 DR2 typical [Fe/H] uncertainties for red giant-branch stars. Our Gaussian fit to the Cra2 MDF is represented by the red dashed line. Gray vertical bands illustrate ±1, 2, and 3 times the $\sigma_{[Fe/H]} = 0.28$ (±0.03) dispersion around the $\langle[Fe/H]\rangle = -2.16$ (±0.04) black line. Right: stellar mass–metallicity relation (MZR) for Local Group dwarf galaxies. Visual scheme is the same as Figure 1. Diffuse dwarfs Cra2 (green '⋆' symbol), Antlia 2 (yellow 'X'), and Andromeda 19 (purple '+') are highlighted with metallicities from this work, Ji et al. (2021), and Collins et al. (2020), respectively. Milky Way satellites, M31 satellites, and Local Group field dwarf galaxies are plotted as blue squares, orange triangles, and gray circles, respectively. Chemical information is from Kirby et al. (2013) and Simon (2019), with the exception of the Large and Small Magellanic Clouds (LMC and SMC) for which we take values from Limberg et al. (2022, see text). Absolute V-band magnitude values are from the Pace (2025) compilation. The corresponding stellar masses ($M_\star$) are computed as in Equation 5. We include Cra2's location in the horizontal M_V axis assuming different $M_\star$ loss scenarios (white '⋆' symbols with green edges). The MZR from Kirby et al. (2013) is the black line with ±1, 2, 3, 4, and 5σ scatter as the gray bands.

MZR (Ji et al. 2021, also Section 4.3), and (*iv*) short star formation history (SFH) with quenching $\gtrsim$10 Gyr ago (Walker et al. 2019). We build on these arguments, but incorporate our own findings, to scrutinize possible scenarios for the origin of Cra2's remarkable properties and, by extension, Ant2 and And19 as well. We also consider that (*v*) Cra2 is unmistakably tidally disrupting (Figures 2 and 4), including our detection of a stellar stream around it (also Coppi et al. 2024), and (*vi*) the evidence that a cuspy NFW halo with fiducial concentration is unlikely to reproduce the system's kinematics with reasonable initial mass (Figure 6 and Section 4.2, as well as previous works; Sanders et al. 2018; Fu et al. 2019; Borukhovetskaya et al. 2022; Errani et al. 2022). Below, we consider if proposed formation pathways can fulfill this set of criteria.

5.1. *Dry mergers*

According to Collins et al. (2022), merger activity could be a mechanism to form And19 and, for the sake of the present discussion, the other diffuse dwarfs Cra2 and Ant2. These authors argued that dry mergers could naturally produce both the unusual structural properties of And19 and its low metallicity. In their hypothesis, the building blocks of And19, hence Cra2 and Ant2, would have been UFD galaxies since these are very metal-poor systems ($\langle[Fe/H]\rangle < -2$, see MZR in Figure 7) commensurate with the diffuse dwarfs. Interestingly, since UFDs are essentially reionization fossils quenched at high redshift (e.g., Weisz et al. 2014), this proposition would automatically explain the exquisitely old stellar populations of Cra2, And19, and Ant2. Simulation work by Orkney et al. (2021) has also claimed that late minor mergers could produce constant-density cores in dwarf galaxies of similar mass to Cra2 and And19.

Indeed, galaxies in the mass range of Cra2 ($M_\star \sim 3 \times 10^5\, M_\odot$) and Ant2 ($M_\star \sim 10^6\, M_\odot$; $M_V = -9.7$ in Equation 5) are expected to have experienced $\mathcal{O}(10)$ accretion events with even smaller systems (e.g., Griffen et al. 2018). However, the same is true for all other classical MW satellites of similar luminosity such as Draco and Sculptor dSph galaxies and, therefore, it is difficult to invoke dry mergers as the sole responsible for the

extreme properties of diffuse dwarfs. In any case, we mention this possibility since it can actually be tested with detailed chemical abundances for stars in the MW diffuse satellites. Collins et al. (2022) suggested this possibility in the context of And19, but this galaxy is too distant (∼800 kpc; Savino et al. 2022), hence its stars are too faint, for this kind of study with current instrumentation. Nevertheless, the most luminous RGB stars in Cra2 and Ant2 (∼120–140 kpc) are bright enough (DECam $g \sim 18.5$) that they are amenable to high-resolution spectroscopy ($\mathcal{R} \geq 20{,}000$) from the ground with 6–8 m-class telescopes. More specifically, a lack of neutron-capture elements is a defining feature of UFDs (Ji et al. 2019; Simon 2019) and can be used as a diagnostic.

5.2. *Star formation and supernovae feedback*

We have shown that a plausible explanation to the large velocity dispersion ratio between Cra2's stellar stream and remnant body is a cored halo with small core radius. Bursty star formation is usually accepted as the culprit for the core-cusp transformation in relatively bright ($M_\star \gtrsim 10^7\,M_\odot$) dwarf galaxies (see reviews by Bullock & Boylan-Kolchin 2017 and Sales et al. 2022). In this process, supernovae outflows transport the central gas outward and the associated gravitational potential fluctuations transfer energy to the collisionless dark matter particles, which end up in dynamically-hotter (higher-energy) orbits at larger radii (Navarro et al. 1996a; Read & Gilmore 2005; Pontzen & Governato 2012; Brooks & Zolotov 2014; El-Zant et al. 2016; Read et al. 2016).

The effectiveness of the above-described feedback-induced core creation mechanism depends on the amount of energy to be injected into the galaxy's interstellar medium (the number of supernovae $\propto M_\star$) and the total dark matter mass that needs to be moved around ($\propto$ halo mass M_h), i.e., fundamentally the stellar-to-halo mass ratio ($M_\star/M_\mathrm{h}$, Peñarrubia et al. 2012; Di Cintio et al. 2014). Hydrodynamical simulations converge on a threshold where feedback becomes inefficient at producing cores of $\log(M_\star/M_\mathrm{h}) \lesssim -3.5$ (Tollet et al. 2016; Fitts et al. 2017; Benítez-Llambay et al. 2019), which translates to $M_\star \lesssim 10^6\,M_\odot$ using the empirical abundance matching relation from Rodríguez-Puebla et al. (2017), which is about the $M_\star$ of Sculptor dSph as well as Ant2.

Following the above-cited premise of abundance matching (from Rodríguez-Puebla et al. 2017), the expectation for a galaxy of Cra2's $M_\star$ is $\log(M_\star/M_\mathrm{h}) \approx -4.0$ prior to tidal disruption, which is well within the regime where core creation is not expected, at least via bursty star formation and supernovae feedback. We find almost identical values for $M_\star/M_\mathrm{h}$ using the dwarf-galaxy specific present-day (redshift $z < 0.05$) stellar-to-halo mass relation from Kado-Fong et al. (2025) and the MW-tailored galaxy–halo connection prescription from Nadler et al. (2020). It is unclear, however, if we should consider the stellar-to-halo mass relation at redshift $z \sim 0$ or at the moment of Cra2's quenching ∼10.5 Gyr ago ($z = 2$ in Planck Collaboration et al. 2020 cosmology). If we adopt the latter, $\log(M_\star/M_\mathrm{h}) \approx -3.9$ for Cra2. In the most optimistic case, where we, again, compensate for 50% $M_\star$ loss in Cra2, we can bring it to $\log(M_\star/M_\mathrm{h}) \approx -3.7$ at redshift $z = 2$.

In addition to high $M_\star/M_\mathrm{h}$, recent works have pointed out that multiple cycles of star formation, i.e., a prolonged SFH of $\gtrsim$8 Gyr (Read et al. 2019; Muni et al. 2025) are also required to form a dark matter core. Due to the early quenching of And19, Collins et al. (2022) argued against a cored halo in that galaxy, a reasoning that also applies to Cra2. Having said that, we note that Sculptor dSph also experienced a short SFH (Kirby et al. 2011; de Boer et al. 2012; Vincenzo et al. 2016; Bettinelli et al. 2019; de los Reyes et al. 2022) and there are claims that this galaxy has a cored halo (Battaglia et al. 2008; Walker & Peñarrubia 2011; Amorisco & Evans 2012; Agnello & Evans 2012, but see Strigari et al. 2010, 2017 and Vitral et al. 2025). Hence, confirming the true shape the dark matter density profile in Sculptor dSph with larger kinematic data sets will also be important to better constrain the core-cusp transformation process.

To summarize, the situation is the following. Given the low $M_\star$, hence low $M_\star/M_\mathrm{h}$ from abundance matching, and early quenching of Cra2, star formation and supernovae feedback should be insufficient to significantly reduce the central dark matter density and convert a cuspy NFW halo into a cored one. This line of reasoning might disfavor the cored halo hypothesis for Cra2, thus supporting a low-concentration NFW profile. However, the plausibility of this scenario largely depends on the scatter of the mass–concentration relation in the low-mass regime, which is difficult to constrain given the limiting resolution in cosmological simulations. Another justification for a low-concentration halo could be warm dark matter, which naturally predicts low-mass halos to be less concentrated than CDM ones (e.g., Macciò et al. 2013; Ludlow et al. 2016, and references therein). Having said that, if one is to invoke an interpretation outside collisionless CDM, solutions that would naturally produce a low-density central core have also been proposed for Cra2, including, e.g., self-interacting dark matter (Zhang et al. 2024).

5.3. *High gas fraction and ram-pressure stripping*

Although stellar/supernovae feedback is typically assumed to be responsible for gas removal in dwarf galaxies, hence gravitational potential variations and redistribution of dark matter particles, other baryonic processes could, in principle, be responsible for the destruction of central cusps (see discussion by Li et al. 2023). Based on observations of bright post-starburst dwarfs ($10^8 < M_\star/M_\odot \lesssim 10^9$, similar to LMC and SMC) containing tails of stripped material in both galaxy clusters and groups, Grishin et al. (2021) proposed that gas removal via ram-pressure stripping could be responsible for the formation of low-mass UDGs. In this scenario, ram pressure would both induce a star-formation burst, followed by quick quenching, and fast change in the gravitational potential due to gas loss accompanied by considerable expansion.

The collective of diffuse dwarfs in the Local Group, for which Cra2 is now the best-studied exemplar, could represent a more extreme version of the "future-UDGs" analyzed by Grishin et al. (2021). In the case of an initially high gas fraction, in comparison to the average atomic hydrogen (HI) mass–$M_\star$ scaling relation (Huang et al. 2012; Guo et al. 2021), a large portion of these galaxies' total mass would be susceptible to ram-pressure stripping. During infall into the Local Group, the interaction with the MW's or M31's hot corona (i.e., their circumgalactic medium, Tumlinson et al. 2017) could have stripped the gas content from these galaxies (e.g., Nichols & Bland-Hawthorn 2011). Then, the associated gravitational potential variations, combined with tides, would have transformed the structural properties of these galaxies into their current diffuse status (see also Wang et al. 2024a).

We finish by saying that the above-described hypothesis of high gas fraction combined with ram-pressure stripping is consistent with the low metallicity of Cra2 and other diffuse dwarfs (Ant2, And19). Since the number of supernovae occurring in a galaxy is proportional to its $M_\star$, the excess of gas would provide extra material to dilute metals into, diminishing the overall metallicity of these systems. This is similar to how star-formation rate (i.e., gas availability; Kennicutt 1998) is anti-correlated with metallicity in the fundamental MZR (Mannucci et al. 2010; Maiolino & Mannucci 2019). Future high-resolution hydrodynamical simulations should be able to test our conjectures.

6. CONCLUSIONS

Below, we list our main results from the analysis of S^5 DR2 data in the fields around Crater 2 (Cra2). Then, we close the paper with a high-level summary paragraph.

- Within the S^5 program (Li et al. 2019), we performed spectroscopic observations across 14 fields of $\sim$3 deg^2 each around the diffuse MW dSph satellite Cra2 using 2dF+AAOmega. Out of these, 1100 genuine stars with good-quality data were considered for Cra2 membership (Appendix A).

- We computed N-body models for the Cra2 system including a realistic past orbit in the combined potential of the MW and LMC. The simulations can broadly reproduce the properties of the Cra2 stellar stream, including a distance gradient of $-4.9\,\mathrm{kpc\,deg^{-1}}$ that matches the distribution of variable RR Lyrae stars discovered by Coppi et al. (2024) and a velocity gradient consistent with the measurement from S^5 DR2 data.

- We fitted kinematics and chemistry of the Cra2 galaxy and stream with a Bayesian mixture modeling approach. Our results for the galaxy's main body are compatible with previous measurements, including a systemic line-of-sight velocity in the Galactic standard of rest frame of $v_\mathrm{gsr} = -81.2 \pm 0.3\,\mathrm{km\,s^{-1}}$ (heliocentric $v_\mathrm{hel} = +89.2 \pm 0.3\,\mathrm{km\,s^{-1}}$), central line-of-sight velocity dispersion of $\sigma_{v,\mathrm{gal}} = 2.51^{+0.33}_{-0.30}\,\mathrm{km\,s^{-1}}$, and mean central metallicity of $\langle[\mathrm{Fe/H}]\rangle = -2.16 \pm 0.04$. Previous works could not measure a velocity gradient, whereas we found a $\approx 7\sigma$ detection of $-4.5 \pm 0.6\,\mathrm{km\,s^{-1}\,deg^{-1}}$ along the Cra2 system.

- We identified 143 Cra2 red giant-branch (RGB) members at probability $P > 50\%$ within the S^5 DR2 footprint, including stars as far as $10 \times$ Cra2's angular $R_{1/2}$, which translates to $\gtrsim$20 kpc physical separation after accounting for the distance gradient. We formally classified 114 of these RGB stars as central members of the Cra2 galaxy and 29 as part of the stream. We then estimated a lower limit for Cra2's stellar mass loss of $21 \pm 7\%$.

- Inspired by Errani et al. (2015), we measured the velocity dispersion ratio between the Cra2 stream and central remnant to be $\sigma_{v,\mathrm{str}}/\sigma_{v,\mathrm{gal}} = 2.30^{+0.41}_{-0.35}$. We found that this observation is difficult to conciliate with an NFW cuspy halo with fiducial concentration and reasonable initial mass from abundance matching. Instead, either a cored halo with small core radius (see Section 3.1) or a low-concentration NFW model can reproduce this ratio. Despite that, additional N-body simulations will certainly be required to exactly match all phase-space properties of Cra2.

- Contrary to the expectation for a galaxy that has experienced tidal stripping (Riley et al. 2025), we found that Cra2 is $\approx 1.5\sigma$ metal-poor compared to the Kirby et al. (2013) Local Group stellar mass–metallicity relation (MZR). Compensating for 50/90/99% stellar mass loss brings this tension with the MZR to the $2/3/5\sigma$ level. We concluded that tidal disruption and low metallicity are not mutually exclusive in diffuse dwarfs such as Cra2 (also Antlia 2 and Andromeda 19).

This paper demonstrates the power of spectroscopic observations at large radii around dwarf galaxies in the Local Group. We have shown that the diffuse Milky Way satellite Cra2 is undeniably experiencing tidal disruption and has a lower-than-expected metallicity in comparison to the MZR. Moreover, we have provided evidence that an NFW cuspy halo with fiducial concentration struggles to reproduce the combined kinematics of the Cra2 galaxy and stellar stream with reasonable halo mass from abundance matching. In the future, tidal tails might be key to explore the dark matter content in MW satellites from yet-to-be discovered low-surface brightness features around them. Also, future theoretical work must be able to fully replicate the properties of Cra2 and its siblings Antlia 2 and Andromeda 19. Otherwise, this emerging population of diffuse dwarf galaxies could represent a novel small-scale challenge to galaxy formation models and, perhaps, point to physics beyond the collisionless cold dark matter theory.

Software: `Anaconda` (Anaconda Software Distribution 2020), `CMasher` (van der Velden 2020), `corner` (Foreman-Mackey 2016), `gala` (Price-Whelan 2017), `jupyter` (Kluyver et al. 2016), `matplotlib` (Hunter 2007), `NumPy` (van der Walt et al. 2011), `pandas` (McKinney 2010), `SciPy` (Virtanen et al. 2020), `scikit-learn` (Pedregosa et al. 2012), `TOPCAT` (Taylor 2005).

This work is part of the ongoing S^5 program (https://s5collab.github.io). S^5 includes data obtained with the Anglo-Australian Telescope in Australia. We acknowledge the traditional owners of the land on which the AAT stands, the Gamilaraay people, and pay our respects to elders past and present.

G.L. acknowledges funding from KICP/UChicago through a KICP Postdoctoral Fellowship. G.L. is indebted to all those involved with the multi-institutional *Milky Way BR* Group for the weekly discussions. G.L. also thanks Evan Kirby, Cristina Chiappini, and Marcel Pawlowski for useful comments during visits to University of Notre Dame/USA and to Leibniz-Institut für Astrophysik Potsdam/Germany as well as Chin Yi Tan for conversations over many coffee breaks and meetings at KICP. A.P.J. acknowledges support from the National Science Foundation under grant AST-2307599 and the Alfred P. Sloan Research Fellowship. T.S.L. acknowledges financial support from Natural Sciences and Engineering Research Council of Canada (NSERC) through grant RGPIN-2022-04794. D.E. thanks Eugene Vasiliev for helpful discussions on `AGAMA`. S.K. acknowledges support from the Science & Technology Facilities Council (STFC) grant ST/Y001001/1. S.L.M. acknowledges support from ARC DP220102254 and the UNSW Scientia Fellowship program.

This work has made use of data from the European Space Agency (ESA) mission *Gaia* (https://www.cosmos.esa.int/gaia), processed by the *Gaia* Data Processing and Analysis Consortium (DPAC, https://www.cosmos.esa.int/web/gaia/dpac/consortium). Funding for the DPAC has been provided by national institutions, in particular the institutions participating in the *Gaia* Multilateral Agreement.

This work also made use of DELVE survey data. The DELVE project is partially supported by the NASA Fermi Guest Investigator Program Cycle 9 No. 91201. This work is partially supported by Fermilab LDRD project L2019-011. This material is based upon work supported by the National Science Foundation under Grant No. AST-2108168, AST-2108169, AST2307126, and AST-2407526.

This paper also made use of the Whole Sky Database (wsdb) created by Sergey Koposov and maintained at the Institute of Astronomy, Cambridge by Sergey Koposov, Vasily Belokurov, and Wyn Evans with financial support from the Science & Technology Facilities Council (STFC) and the European Research Council (ERC).

This research has made use of the VizieR catalogue access tool, CDS, Strasbourg, France (https://cds.u-strasbg.fr). The original description of the VizieR service was published in Ochsenbein et al. (2000).

REFERENCES

Abdurro'uf, Accetta, K., Aerts, C., et al. 2022, ApJS, 259, 35 13

Agnello, A., & Evans, N. W. 2012, ApJL, 754, L39 15

Amorisco, N. C. 2019, MNRAS, 489, L22 2, 12, 13

Amorisco, N. C., & Evans, N. W. 2012, MNRAS, 419, 184 15

Anaconda Software Distribution. 2020, Anaconda Software Distribution, v24.3.0, Anaconda Inc. https://docs.anaconda.com/ 17

Applebaum, E., Brooks, A. M., Christensen, C. R., et al. 2021, ApJ, 906, 96 2, 13

Arroyo-Polonio, J. M., Battaglia, G., Thomas, G. F., et al. 2024, A&A, 692, A195 12

Astropy Collaboration, Robitaille, T. P., Tollerud, E. J., et al. 2013, A&A, 558, A33 5

Astropy Collaboration, Price-Whelan, A. M., Sipőcz, B. M., et al. 2018, AJ, 156, 123 5

Awad, P., Li, T. S., Erkal, D., et al. 2025, A&A, 693, A69 7, 8

Barbosa, F. O., Chiti, A., Limberg, G., et al. 2025, arXiv e-prints, arXiv:2504.03593 13

Battaglia, G., Helmi, A., Tolstoy, E., et al. 2008, ApJL, 681, L13 15

Battaglia, G., & Nipoti, C. 2022, NatAs, 6, 659 2

Battaglia, G., Taibi, S., Thomas, G. F., & Fritz, T. K. 2022, A&A, 657, A54 8

Behroozi, P., Wechsler, R. H., Hearin, A. P., & Conroy, C. 2019, MNRAS, 488, 3143 7

Behroozi, P. S., Wechsler, R. H., & Conroy, C. 2013, ApJ, 770, 57 7

Benavides, J. A., Sales, L. V., Abadi, M. G., et al. 2023, MNRAS, 522, 1033 3

Benítez-Llambay, A., Frenk, C. S., Ludlow, A. D., & Navarro, J. F. 2019, MNRAS, 488, 2387 15

Bennett, M., & Bovy, J. 2019, MNRAS, 482, 1417 5

Bettinelli, M., Hidalgo, S. L., Cassisi, S., et al. 2019, MNRAS, 487, 5862 15

Borukhovetskaya, A., Navarro, J. F., Errani, R., & Fattahi, A. 2022, MNRAS, 512, 5247 2, 14

Bovy, J. 2015, ApJS, 216, 29 5

Brooks, A. M., & Zolotov, A. 2014, ApJ, 786, 87 15

Bullock, J. S., & Boylan-Kolchin, M. 2017, ARA&A, 55, 343 2, 15

Caldwell, N., Walker, M. G., Mateo, M., et al. 2017, ApJ, 839, 20 2, 7, 13

Carleton, T., Errani, R., Cooper, M., et al. 2019, MNRAS, 485, 382 3

Collins, M. L. M., Tollerud, E. J., Rich, R. M., et al. 2020, MNRAS, 491, 3496 2, 13, 14

Collins, M. L. M., Williams, B. F., Tollerud, E. J., et al. 2022, MNRAS, 517, 4382 2, 13, 14, 15

Coppi, P. S., Zinn, R., Baltay, C., et al. 2024, MNRAS, arXiv:2402.01899 3, 4, 5, 6, 7, 8, 10, 11, 14, 16

Cullinane, L. R., Gilbert, K. M., Escala, I., et al. 2024, arXiv e-prints, arXiv:2407.04349 13

Cunningham, E. C., Hunt, J. A. S., Price-Whelan, A. M., et al. 2024, ApJ, 963, 95 13

Dalal, N., & Kravtsov, A. 2022, PhRvD, 106, 063517 2

Danieli, S., Greene, J. E., Carlsten, S., et al. 2023, ApJ, 956, 6 7, 12

de Blok, W. J. G. 2010, Advances in Astronomy, 2010, 789293 2

de Boer, T. J. L., Tolstoy, E., Hill, V., et al. 2012, A&A, 539, A103 15

de los Reyes, M. A. C., Kirby, E. N., Ji, A. P., & Nuñez, E. H. 2022, ApJ, 925, 66 15

Di Cintio, A., Brook, C. B., Dutton, A. A., et al. 2017, MNRAS, 466, L1 3

Di Cintio, A., Brook, C. B., Macciò, A. V., et al. 2014, MNRAS, 437, 415 15

Dotter, A., Chaboyer, B., Jevremović, D., et al. 2008, ApJS, 178, 89 10

Drimmel, R., & Poggio, E. 2018, Research Notes of the American Astronomical Society, 2, 210 5

Drlica-Wagner, A., Bechtol, K., Mau, S., et al. 2020, ApJ, 893, 47 2

Drlica-Wagner, A., Carlin, J. L., Nidever, D. L., et al. 2021, ApJS, 256, 2 5

Drlica-Wagner, A., Ferguson, P. S., Adamów, M., et al. 2022, ApJS, 261, 38 5, 10, 11, 22

Dutton, A. A., & Macciò, A. V. 2014, MNRAS, 441, 3359 6, 12

El-Zant, A. A., Freundlich, J., & Combes, F. 2016, MNRAS, 461, 1745 15

Erkal, D., Belokurov, V., Laporte, C. F. P., et al. 2019, MNRAS, 487, 2685 5

Errani, R., Navarro, J. F., Ibata, R., & Peñarrubia, J. 2022, MNRAS, 511, 6001 2, 14

Errani, R., Penarrubia, J., & Tormen, G. 2015, MNRAS, 449, L46 2, 10, 11, 13, 16

Errani, R., Walker, M. G., Rozier, S., Peñarrubia, J., & Navarro, J. F. 2025, ApJ, 992, 162 11

Evans, D. W., Riello, M., De Angeli, F., et al. 2018, A&A, 616, A4 5

Fattahi, A., Navarro, J. F., Frenk, C. S., et al. 2018, MNRAS, 476, 3816 2, 13

Fitts, A., Boylan-Kolchin, M., Elbert, O. D., et al. 2017, MNRAS, 471, 3547 15

Flaugher, B., Diehl, H. T., Honscheid, K., et al. 2015, AJ, 150, 150 5
Foreman-Mackey, D. 2016, JOSS, 1, 24 17
Foreman-Mackey, D., Hogg, D. W., Lang, D., & Goodman, J. 2013, PASP, 125, 306 8, 12
Fritz, T. K., Battaglia, G., Pawlowski, M. S., et al. 2018, A&A, 619, A103 5, 8
Fu, S. W., Simon, J. D., & Alarcón Jara, A. G. 2019, ApJ, 883, 11 2, 7, 11, 13, 14
Gaia Collaboration, Prusti, T., de Bruijne, J. H. J., et al. 2016, A&A, 595, A1 4
Gaia Collaboration, Brown, A. G. A., Vallenari, A., et al. 2018, A&A, 616, A1 5
—. 2021, A&A, 649, A1 5
Gaia Collaboration, Vallenari, A., Brown, A. G. A., et al. 2023, A&A, 674, A1 5
Gannon, J. S., Ferré-Mateu, A., Forbes, D. A., et al. 2024, MNRAS, 531, 1856 3
Garrison-Kimmel, S., Bullock, J. S., Boylan-Kolchin, M., & Bardwell, E. 2017, MNRAS, 464, 3108 7, 12
Gravity Collaboration, Abuter, R., Amorim, A., et al. 2018, A&A, 615, L15 5
Griffen, B. F., Dooley, G. A., Ji, A. P., et al. 2018, MNRAS, 474, 443 14
Grishin, K. A., Chilingarian, I. V., Afanasiev, A. V., et al. 2021, Nature Astronomy, 5, 1308 16
Guo, H., Jones, M. G., Wang, J., & Lin, L. 2021, ApJ, 918, 53 16
Hayes, C. R., Majewski, S. R., Hasselquist, S., et al. 2020, ApJ, 889, 63 2, 13
Hu, W., Barkana, R., & Gruzinov, A. 2000, PhRvL, 85, 1158 2
Huang, S., Haynes, M. P., Giovanelli, R., & Brinchmann, J. 2012, ApJ, 756, 113 16
Hunter, J. D. 2007, Computing in Science and Engineering, 9, 90 17
Husser, T. O., Wende-von Berg, S., Dreizler, S., et al. 2013, A&A, 553, A6 5
Jethwa, P., Erkal, D., & Belokurov, V. 2018, MNRAS, 473, 2060 7, 12
Ji, A. P., Simon, J. D., Frebel, A., Venn, K. A., & Hansen, T. T. 2019, ApJ, 870, 83 15
Ji, A. P., Koposov, S. E., Li, T. S., et al. 2021, ApJ, 921, 32 2, 4, 6, 7, 8, 9, 11, 13, 14
Kado-Fong, E., Mao, Y.-Y., Asali, Y., et al. 2025, arXiv e-prints, arXiv:2509.20444 7, 12, 15
Kahlhoefer, F., Kaplinghat, M., Slatyer, T. R., & Wu, C.-L. 2019, JCAP, 2019, 010 2
Kallivayalil, N., van der Marel, R. P., Besla, G., Anderson, J., & Alcock, C. 2013, ApJ, 764, 161 6
Kennicutt, Robert C., J. 1998, ApJ, 498, 541 16
Kirby, E. N., Cohen, J. G., Guhathakurta, P., et al. 2013, ApJ, 779, 102 2, 13, 14, 17
Kirby, E. N., Cohen, J. G., Smith, G. H., et al. 2011, ApJ, 727, 79 15
Kluyver, T., Ragan-Kelley, B., Pérez, F., et al. 2016, in Positioning and Power in Academic Publishing: Players, Agents and Agendas, ed. F. Loizides & B. Schmidt (Amsterdam: IOS Press), 87 17
Koda, J., Yagi, M., Yamanoi, H., & Komiyama, Y. 2015, ApJL, 807, L2 2
Kong, D., Kaplinghat, M., Yu, H.-B., Fraternali, F., & Mancera Piña, P. E. 2022, ApJ, 936, 166 3
Koposov, S., Belokurov, V., Evans, N. W., et al. 2008, ApJ, 686, 279 2
Koposov, S. E. 2019, RVSpecFit: Radial velocity and stellar atmospheric parameter fitting, Astrophysics Source Code Library, record ascl:1907.013, , 5
Koposov, S. E., Rix, H.-W., & Hogg, D. W. 2010, ApJ, 712, 260 7
Koposov, S. E., Gilmore, G., Walker, M. G., et al. 2011, ApJ, 736, 146 5
Koposov, S. E., Erkal, D., Li, T. S., et al. 2023, MNRAS, 521, 4936 5
Lewis, I. J., Cannon, R. D., Taylor, K., et al. 2002, MNRAS, 333, 279 3
Li, T. S., Simon, J. D., Kuehn, K., et al. 2018, ApJ, 866, 22 7
Li, T. S., Koposov, S. E., Zucker, D. B., et al. 2019, MNRAS, 490, 3508 3, 4, 5, 16
Li, T. S., Koposov, S. E., Erkal, D., et al. 2021, ApJ, 911, 149 5
Li, T. S., Ji, A. P., Pace, A. B., et al. 2022, ApJ, 928, 30 3, 5, 7
Li, Z., Dekel, A., Mandelker, N., Freundlich, J., & François, T. L. 2023, MNRAS, 518, 5356 16
Limberg, G., Souza, S. O., Pérez-Villegas, A., et al. 2022, ApJ, 935, 109 13, 14
Limberg, G., Queiroz, A. B. A., Perottoni, H. D., et al. 2023, ApJ, 946, 66 13
Lovell, M. R., & Zavala, J. 2023, MNRAS, 520, 1567 2
Ludlow, A. D., Bose, S., Angulo, R. E., et al. 2016, MNRAS, 460, 1214 15
Macciò, A. V., Ruchayskiy, O., Boyarsky, A., & Muñoz-Cuartas, J. C. 2013, MNRAS, 428, 882 15
Maiolino, R., & Mannucci, F. 2019, A&A Rv, 27, 3 16
Majewski, S. R., Skrutskie, M. F., Weinberg, M. D., & Ostheimer, J. C. 2003, ApJ, 599, 1082 7
Majewski, S. R., Schiavon, R. P., Frinchaboy, P. M., et al. 2017, AJ, 154, 94 13

Mancera Piña, P. E., Fraternali, F., Adams, E. A. K., et al. 2019, ApJL, 883, L33 3
Mannucci, F., Cresci, G., Maiolino, R., Marconi, A., & Gnerucci, A. 2010, MNRAS, 408, 2115 16
Manwadkar, V., & Kravtsov, A. V. 2022, MNRAS, 516, 3944 7, 12
Martin, N. F., de Jong, J. T. A., & Rix, H.-W. 2008, ApJ, 684, 1075 7
McConnachie, A. W., Huxor, A., Martin, N. F., et al. 2008, ApJ, 688, 1009 2
McGaugh, S. S. 2016, ApJL, 832, L8 2
McKinney, W. 2010, in Proceedings of the 9th Python in Science Conference, ed. Stéfan van der Walt & Jarrod Millman, 56 17
Milgrom, M. 1983, ApJ, 270, 371 2
Muñoz, R. R., Côté, P., Santana, F. A., et al. 2018, ApJ, 860, 66 2
Muni, C., Pontzen, A., Read, J. I., et al. 2025, MNRAS, 536, 314 15
Nadler, E. O., Yang, D., & Yu, H.-B. 2023, ApJL, 958, L39 3
Nadler, E. O., Wechsler, R. H., Bechtol, K., et al. 2020, ApJ, 893, 48 7, 12, 15
Navarro, J. F., Eke, V. R., & Frenk, C. S. 1996a, MNRAS, 283, L72 15
Navarro, J. F., Frenk, C. S., & White, S. D. M. 1996b, ApJ, 462, 563 2, 5, 6
—. 1997, ApJ, 490, 493 2, 5, 6
Nichols, M., & Bland-Hawthorn, J. 2011, ApJ, 732, 17 16
Nidever, D. L., Hasselquist, S., Hayes, C. R., et al. 2020, ApJ, 895, 88 13
Ochsenbein, F., Bauer, P., & Marcout, J. 2000, A&AS, 143, 23 17
Orkney, M. D. A., Read, J. I., Rey, M. P., et al. 2021, MNRAS, 504, 3509 14
Pace, A. B. 2025, The Open Journal of Astrophysics, 8, 142 3, 9, 13, 14
Pace, A. B., Erkal, D., & Li, T. S. 2022, ApJ, 940, 136 6, 7, 8, 11
Pace, A. B., & Li, T. S. 2019, ApJ, 875, 77 4, 7
Pace, A. B., Kaplinghat, M., Kirby, E., et al. 2020, MNRAS, 495, 3022 12
Peñarrubia, J., Navarro, J. F., & McConnachie, A. W. 2008, ApJ, 673, 226 2
Peñarrubia, J., Pontzen, A., Walker, M. G., & Koposov, S. E. 2012, ApJL, 759, L42 15
Pedregosa, F., Varoquaux, G., Gramfort, A., et al. 2012, arXiv e-prints, arXiv:1201.0490 17
Pietrzyński, G., Graczyk, D., Gieren, W., et al. 2013, Nature, 495, 76 6
Planck Collaboration, Aghanim, N., Akrami, Y., et al. 2020, A&A, 641, A6 6, 15
Plummer, H. C. 1911, MNRAS, 71, 460 6
Pontzen, A., & Governato, F. 2012, MNRAS, 421, 3464 15
Pozo, A., Broadhurst, T., Emami, R., & Smoot, G. 2022, MNRAS, 515, 2624 2
Price-Whelan, A. M. 2017, JOSS, 2, 388 17
Read, J. I., Agertz, O., & Collins, M. L. M. 2016, MNRAS, 459, 2573 6, 12, 15
Read, J. I., & Gilmore, G. 2005, MNRAS, 356, 107 15
Read, J. I., Iorio, G., Agertz, O., & Fraternali, F. 2017, MNRAS, 467, 2019 7
Read, J. I., Walker, M. G., & Steger, P. 2019, MNRAS, 484, 1401 15
Riello, M., De Angeli, F., Evans, D. W., et al. 2020, arXiv e-prints, arXiv:2012.01916 5
Riley, A. H., Bieri, R., Deason, A. J., et al. 2025, arXiv e-prints, arXiv:2509.06859 2, 11, 13, 17
Rodríguez-Puebla, A., Primack, J. R., Avila-Reese, V., & Faber, S. M. 2017, MNRAS, 470, 651 7, 15
Sales, L. V., Wetzel, A., & Fattahi, A. 2022, Nature Astronomy, 6, 897 2, 15
Sanders, J. L., Evans, N. W., & Dehnen, W. 2018, MNRAS, 478, 3879 2, 14
Savino, A., Weisz, D. R., Skillman, E. D., et al. 2022, ApJ, 938, 101 15
Schive, H.-Y., Chiueh, T., & Broadhurst, T. 2014, Nature Physics, 10, 496 2
Schlegel, D. J., Finkbeiner, D. P., & Davis, M. 1998, ApJ, 500, 525 4
Sharp, R., Saunders, W., Smith, G., et al. 2006, in Society of Photo-Optical Instrumentation Engineers (SPIE) Conference Series, Vol. 6269, Ground-based and Airborne Instrumentation for Astronomy, ed. I. S. McLean & M. Iye, 62690G 3
Shipp, N., Drlica-Wagner, A., Balbinot, E., et al. 2018, ApJ, 862, 114 3
Shipp, N., Li, T. S., Pace, A. B., et al. 2019, ApJ, 885, 3 7
Shipp, N., Erkal, D., Drlica-Wagner, A., et al. 2021, ApJ, 923, 149 5
Shipp, N., Panithanpaisal, N., Necib, L., et al. 2023, ApJ, 949, 44 11
Shipp, N., Riley, A. H., Simpson, C. M., et al. 2025, MNRAS, 542, 1109 11
Simard, L., Mendel, J. T., Patton, D. R., Ellison, S. L., & McConnachie, A. W. 2011, ApJS, 196, 11 3
Simon, J. D. 2019, ARA&A, 57, 375 2, 13, 14, 15
Spergel, D. N., & Steinhardt, P. J. 2000, PhRvL, 84, 3760 2
Strigari, L. E., Frenk, C. S., & White, S. D. M. 2010, MNRAS, 408, 2364 15

—. 2017, ApJ, 838, 123 15
Taibi, S., Battaglia, G., Leaman, R., et al. 2022, A&A, 665, A92 7, 12
Tan, C. Y., Drlica-Wagner, A., Pace, A. B., et al. 2025, arXiv e-prints, arXiv:2509.12313 2
Taylor, M. B. 2005, in Astronomical Society of the Pacific Conference Series, Vol. 347, Astronomical Data Analysis Software and Systems XIV, ed. P. Shopbell, M. Britton, & R. Ebert, 29 17
Tollet, E., Macciò, A. V., Dutton, A. A., et al. 2016, MNRAS, 456, 3542 15
Tolstoy, E., Hill, V., & Tosi, M. 2009, ARA&A, 47, 371 2
Torrealba, G., Koposov, S. E., Belokurov, V., & Irwin, M. 2016, MNRAS, 459, 2370 2, 4, 6, 7, 8, 9, 13
Torrealba, G., Belokurov, V., Koposov, S. E., et al. 2019, MNRAS, 488, 2743 2
Tumlinson, J., Peeples, M. S., & Werk, J. K. 2017, ARA&A, 55, 389 16
van der Burg, R. F. J., Hoekstra, H., Muzzin, A., et al. 2017, A&A, 607, A79 3
van der Marel, R. P., Alves, D. R., Hardy, E., & Suntzeff, N. B. 2002, AJ, 124, 2639 6
van der Marel, R. P., & Kallivayalil, N. 2014, ApJ, 781, 121 5
van der Velden, E. 2020, JOSS, 5, 2004. https://doi.org/10.21105/joss.02004 17
van der Walt, S., Colbert, S. C., & Varoquaux, G. 2011, Computing in Science and Engineering, 13, 22 17
van Dokkum, P. G., Abraham, R., Merritt, A., et al. 2015, ApJL, 798, L45 2, 3
Vasiliev, E. 2019, MNRAS, 482, 1525 5
Vasiliev, E., Belokurov, V., & Erkal, D. 2021, MNRAS, 501, 2279 5, 6
Vincenzo, F., Matteucci, F., de Boer, T. J. L., Cignoni, M., & Tosi, M. 2016, MNRAS, 460, 2238 15
Virtanen, P., Gommers, R., Oliphant, T. E., et al. 2020, NatMe, 17, 261 17
Vitral, E., van der Marel, R. P., Sohn, S. T., et al. 2025, arXiv e-prints, arXiv:2508.20711 15
Vivas, A. K., Walker, A. R., Martínez-Vázquez, C. E., et al. 2020, MNRAS, 492, 1061 9
Walker, A. R., Martínez-Vázquez, C. E., Monelli, M., et al. 2019, MNRAS, 490, 4121 2, 10, 14
Walker, M. G., Mateo, M., Olszewski, E. W., Sen, B., & Woodroofe, M. 2009, AJ, 137, 3109 7
Walker, M. G., McGaugh, S. S., Mateo, M., Olszewski, E. W., & Kuzio de Naray, R. 2010, ApJL, 717, L87 2
Walker, M. G., & Peñarrubia, J. 2011, ApJ, 742, 20 15
Walker, M. G., Mateo, M., Olszewski, E. W., et al. 2016, ApJ, 819, 53 7
Wang, J., Hammer, F., Yang, Y., et al. 2024a, MNRAS, 527, 7144 16
Wang, Y., Nadler, E. O., Mao, Y.-Y., et al. 2024b, ApJ, 976, 119 7
Wechsler, R. H., & Tinker, J. L. 2018, ARA&A, 56, 435 2
Weisz, D. R., Dolphin, A. E., Skillman, E. D., et al. 2014, ApJ, 789, 147 14
Willmer, C. N. A. 2018, ApJS, 236, 47 13
Wilson, E. B. 1927, Journal of the American Statistical Association, 22, 209. https://www.tandfonline.com/doi/abs/10.1080/01621459.1927.10502953 9
Woo, J., Courteau, S., & Dekel, A. 2008, MNRAS, 390, 1453 2
Zhang, X., Yu, H.-B., Yang, D., & An, H. 2024, ApJL, 968, L13 2, 15

APPENDIX

A. DATA TABLE

In Table 3, we present the 1100 stars with good-quality data (see Section 2) used for membership evaluation. The P column shows the membership probability computed with the mixture modeling approach in this work (Section 3.3), while other quantities are taken from the S^5 DR2 catalog.

Table 3. S^5 DR2 data around the Crater 2 galaxy and stream footprint

Gaia DR3 `source_id`	α (deg)	δ (deg)	$\mu_\alpha \cos\delta$ (mas yr^{-1})	μ_δ (mas yr^{-1})	$g^\dagger$	$r^\dagger$	$v_{\rm hel}$ (km s^{-1})	$e_{v_{\rm hel}}$	[Fe/H]	$e_{\rm [Fe/H]}$	P	S/N
3544474297064516096	172.30925	−21.31763	−0.064	0.234	17.15	16.47	17.64	2.94	−2.35	0.25	0.00	5.9
3544502648144931968	172.34935	−20.92886	−0.471	−0.603	17.15	16.46	288.63	2.49	−1.71	0.16	0.00	8.5
3541353230230311552	172.52798	−21.76984	0.354	−0.69	19.20	18.47	−1.86	4.65	−0.69	0.35	0.00	3.6
3544591979168107392	172.55615	−20.38967	−0.210	−0.167	18.62	17.69	47.17	3.09	−0.78	0.33	0.00	5.2
3544973926316400128	172.58195	−20.21502	0.064	−1.107	20.00	18.96	−1.51	6.06	−1.36	0.94	0.00	4.8
3541452907830980736	172.60148	−21.54574	−0.102	−0.002	18.86	18.15	286.68	1.49	−2.08	0.18	0.00	9.6
3544510615308138496	172.64702	−20.95267	−0.271	−0.083	18.64	18.07	129.16	4.85	−2.17	0.33	0.92	5.3
3541455145508547456	172.67600	−21.46399	−0.505	−0.547	20.39	19.18	49.30	7.33	−2.47	0.66	0.00	4.2
3544512749906827904	172.69912	−20.87969	1.208	−0.435	20.48	19.33	12.03	4.98	−1.42	0.65	0.00	3.0

†DECam g and r photometry reported in DELVE DR2 (Drlica-Wagner et al. 2022).
The first 10 rows of this table are shown here to exemplify its format and content.